CHALMERS
UNIVERSITY OF TECHNOLOGY

Mechanical performance and material characterization of secondary aluminum alloys for automotive megacasting

Master's Thesis in Materials Engineering

JIHUI YANG

NITHIN TEJA BANAVATHI MARUTISHA

DEPARTMENT OF INDUSTRIAL AND MATERIALS SCIENCE

CHALMERS UNIVERSITY OF TECHNOLOGY
Gothenburg, Sweden 2025
www.chalmers.se

MASTER'S THESIS 2025

Mechanical performance and material characterization of secondary aluminum alloys for automotive megacasting

JIHUI YANG

NITHIN TEJA BANAVATHI MARUTISHA

CHALMERS
UNIVERSITY OF TECHNOLOGY

DEPARTMENT OF INDUSTRIAL AND MATERIALS SCIENCE
Chalmers University of Technology
Gothenburg, Sweden 2025

Mechanical performance and material characterization of secondary aluminum alloys for automotive megacasting
JIHUI YANG

NITHIN TEJA BANAVATHI MARUTISHA

Supervisor: Anton Hvitt Hultmark, Volvo Cars Corporation
Examiner: Johan Ahlström, Department of Industrial and Materials Science

Master's Thesis 2025
Department of Industrial and Materials Science
Chalmers University of Technology
SE-412 96 Gothenburg
Sweden
Telephone +46 31 772 1000

Cover: Illustration of component that can be made from the mega casting project at Volvo Cars.

Typeset in LaTeX
Gothenburg, Sweden 2025

Mechanical performance and material characterization of secondary aluminum alloys for automotive megacasting

JIHUI YANG, NITHIN TEJA BANAVATHI MARUTISHA
Department of Industrial and Materials Science
Chalmers University of Technology

Abstract

The transition toward sustainable automotive manufacturing has intensified interest in using recycled materials without compromising mechanical performance. This thesis investigates the feasibility of applying secondary aluminum alloys in high-pressure die casting (HPDC), specifically within the megacasting process for large structural components. Four alloy batches were analyzed: one primary aluminum used as the reference (A4), one secondary aluminum with similar chemical composition (B1), and two secondary aluminum variants with different levels of Fe, Cu, Zn, and V (B2–B3). Mechanical performance was evaluated through tensile, three-point bending, and hardness testing, while microstructural analysis, including optical microscopy, metallography, SEM, and X-ray was used to identify shrinkage, porosity, and intermetallic phases.

The results show that recycled aluminum with up to 90% secondary content (B1) can achieve comparable mechanical properties to primary aluminum (A4) when chemical composition remains unchanged. Batches with higher Fe content (B2, B3) exhibited increased yield strength due to solid solution and precipitation strengthening but showed reduced ductility and bending toughness, particularly in regions with greater shrinkage. Comparing the results with historical trials can separate the impact of cast processing and raw material. Microstructural analysis confirmed that casting position influences defect formation and performance. In HPDC, areas farther from the ingate (e.g. F3) generally experience longer flow paths and therefore tend to form more shrinkage and intermetallic phases. Building on this context, this work demonstrates that, with optimized chemistry and process parameters, secondary aluminum alloys can achieve mechanical performance compared with primary alloys, thereby offering a sustainable megacasting solution for the automotive industry.

High-pressure die casting (HPDC); Secondary aluminum; Megacasting; Mechanical performance; Microstructure; Sustainability; Automotive manufacturing

Acknowledgements

This thesis was carried out at Volvo Cars in collaboration with Chalmers University of Technology. We would like to express my deepest gratitude to our academic examiner Johan Ahlström at Chalmers and our industrial supervisor Anton Hvitt Hultmark at Volvo Cars for their invaluable guidance, technical expertise, and continuous support throughout the project. Their feedback and encouragement were instrumental in shaping the direction and outcome of this work.
Special thanks also go to the technicians and engineers in the Volvo materials testing departments for their assistance with sample preparation, testing, and data collection. We are equally grateful to our colleagues, and friends for their support and insightful discussions.

Jihui Yang, Nithin Teja Banavathi Marutisha, Gothenburg, June 2025

Contents

List of Acronyms **xi**

List of Figures **xiii**

List of Tables **xv**

1 Introduction **1**
1.1 Background . . . 1
1.2 Purpose . . . 2
1.3 Limitations . . . 2

2 Theory **5**
2.1 Al-Si alloy . . . 5
2.1.1 Al–Si phase diagram and microstructural formation . . . 5
2.1.2 Microstructural characteristics in Al-Si7 alloy . . . 5
2.1.3 Effect of microstructural features on mechanical testing . . . 8
2.2 Role of alloying elements in aluminum alloys . . . 8
2.2.1 Silicon . . . 9
2.2.2 Magnesium . . . 9
2.2.3 Zinc . . . 9
2.2.4 Copper . . . 10
2.2.5 Iron . . . 10
2.2.6 Manganese . . . 10
2.2.7 Vanadium . . . 10
2.2.8 Strontium . . . 11
2.3 Aluminum alloys usage in automotive industry . . . 11
2.4 Key properties of a body structure part in automotive applications . . . 13
2.4.1 Tensile yield strength, ultimate tensile strength & Young's modulus . . . 13
2.4.2 Bend ductility . . . 14
2.4.3 Hardness . . . 15
2.4.4 Fatigue resistance . . . 15
2.4.5 Corrosion resistance . . . 16
2.5 Challenges in using recycled aluminum for structural castings . . . 17
2.6 High-pressure die casting . . . 19
2.6.1 Mold and die preparation . . . 20
2.6.2 Molten aluminum preparation and injection . . . 20

2.6.3 Solidification, cooling and ejection . . . 21
2.6.4 Trimming, deburring, and surface machining . . . 21
2.6.5 Heat treatment and strengthening . . . 22
2.6.6 Inspection and quality control . . . 23
2.7 The snake tool - R&D test component . . . 24
2.8 Cast trail . . . 25
2.8.1 Process parameter . . . 25
2.8.2 Alloy composition table . . . 26
2.8.3 Challenges during the trails . . . 26

3 Methods 27
3.1 Material selection and sample preparation . . . 27
3.2 Mechanical testing methods . . . 28
3.2.1 Tensile testing . . . 28
3.2.2 Bending testing . . . 29
3.2.3 Hardness testing . . . 30
3.3 Microstructural analysis . . . 32
3.3.1 Optical microscopy . . . 32
3.3.2 Metallography . . . 32
3.3.3 SEM . . . 33
3.3.4 X-ray . . . 34

4 Results 35
4.1 Mechanical testing . . . 35
4.1.1 Tensile testing . . . 35
4.1.2 Bend plate test . . . 38
4.1.2.1 Comparison - Tensile vs. Bending . . . 38
4.1.2.2 Comparison – Flat sample vs Beam structure . . . 40
4.1.3 Hardness test . . . 42
4.2 Fractography of tensile samples . . . 43
4.2.1 Stereo microscopy . . . 43
4.2.2 Metallography . . . 44
4.2.3 Comparison between snake tool and historical cast trial . . . 48
4.2.4 SEM . . . 49
4.2.5 X-ray . . . 51
4.2.6 Effect of chemical composition and process parameters . . . 51
4.2.6.1 Impact of chemical composition . . . 52
4.2.6.2 Impact of process conditions . . . 52

5 Conclusion 53

6 Next Steps & Recommendation 55

References 57

List of Acronyms

Below is the list of acronyms that have been used throughout this thesis listed in alphabetical order:

HPDC	High-Pressure Die Casting
YS	Yield Strength
UTS	Ultimate Tensile Strength
ELVs	End-of-Life Vehicles
EVs	Electric Vehicles
CAGR	Compound Annual Growth Rate
SEM	Scanning Electron Microscopy
BSE	Backscattered Electron
NDT	Non-Destructive Evaluation
LCA	Lifecycle Analysis

List of Figures

2.1 The Al-Si phase diagram 6
2.2 The morphology of α-Al dendrites, eutectic Si, and intermetallic . . . 6
2.3 The morphology of a shrinkage pore 7
2.4 Early prototype design of a rear floor casting 13
2.5 Stress-strain curve 14
2.6 Distribution of bending moment 15
2.7 Illustration of the aluminum life cycle 17
2.8 The general process of HPDC 20
2.9 Three phases of the shot curve in HPDC 21
2.10 Different ways of heat treatment 22
2.11 The design of snake tool 25

3.1 Samples marked for cutting 28
3.2 Tensile sample geometry 29
3.3 3-point bending sample direction 30
3.4 Hardness test zig-zag pattern 31
3.5 Test samples indication 31
3.6 Test samples 32

4.1 Position of flats F1 and F3 in the snake tool 35
4.2 Avg. yield strength results: B1 exhibits a similar yield strength to A4 highlighted in red arrow, while both B2 and B3 show a noticeable increase highlighted in green arrow. 36
4.3 Avg UTS results: A4 and B1 have similar level of UTS. In Flat 1 (F1) highlighted in red arrow, B2 and B3 perform worse in both metrics. However, in Flat 3 (F3), B2 and B3 exhibit the opposite trend highlighted in green arrow 37
4.4 Avg elongation results: A4 and B1 have similar level of elongation highlighted in red arrow. In Flat 1 (F1), B2 and B3 perform worse in both metrics. However, in Flat 3 (F3), B2 and B3 exhibit the opposite trend highlighted in green arrow 37
4.5 Avg YS, UTS and elongation results compared by horizontal and vertical direction samples: vertical samples have similar performance with the previous one. However, for horizontal samples, the UTS and elongation results of B3-T5 are higher than B3-T2, which are different from the previous results. 38

4.6 Bend plate test results: A4 and B1 show consistently higher bending angles at F1, indicating better ductility. B3 exhibit a huge increase in bending angle at F3, showing a position sensitive performance . . . 39
4.7 Tensile test results vs. Bending test results: Both results reflect A4 and B1 have similar performance, B2 and B3 perform relevantly poor. 40
4.8 Comparison of two fracture surface pictures of beam bending samples. 41
4.9 Beam structure 42
4.10 Flat & Beam bending results: Both bending test results show similar trend. 42
4.11 Hardness test results: Similar hardness results within all batches, secondary aluminum content and chemical composition do not affect significantly. 43
4.12 Example for gas porosity and shrinkage porosity 44
4.13 Microscopy pictures of A4 and B1 from F1 and F3 positions with elongation results 44
4.14 Metallography and Fiji pictures of A4 and B1 batch from different positions 46
4.15 Metallography and Fiji pictures of B2 and B3 batch from different positions 47
4.16 Comparison of shrinkage area between snake tool and historical cast trials microstructure 48
4.17 SEM pictures of all batches and different positions, red arrow highlights: porosity, blue arrow highlights: blocky and script scaped phases 50
4.18 X-ray pictures of A4, B1 and B2 batches 51

List of Tables

2.1 Aluminum alloy designation system [29] 12
2.2 Process parameter 25
2.3 Alloy Table 26

3.1 Alloy Table 27
3.2 Tensile test samples 29
3.3 Parameters for three-point bending test 29
3.4 Bend plate test sample 30
3.5 Hardness test sample 31

4.1 Shrinkage area percentage of different samples based on metallographic image analysis 45
4.2 Comparison between Snake tool and historical cast trial 49

1

Introduction

1.1 Background

The automotive industry is undergoing a transformative shift towards sustainable manufacturing practices. It is mainly driven by the need to reduce greenhouse gas emissions and carbon footprint and finally achieve carbon neutrality. Though based on the report from ACEA [1], the CO_2 emissions per car produced dropped 7.4% from 2005 to 2022 in the EU, that is still not enough. Around the world, governments and regulatory bodies have been implementing policies and regulations aimed at reducing emissions in the automotive industry. In the United States, the Biden administration announced new emissions standards for heavy-duty vehicles [2] designed to substantially decrease greenhouse gas emissions. Similarly, the European Union also took ambitious steps to reduce emissions in the automotive sector. Automakers need to reduce 55% CO_2 emission for new cars and 50% for new vans from 2030 to 2034 compared to 2021 levels [3]. As a global manufacturer, Volvo Cars is compelled to innovate in materials and processes to align with these targets.

Large-scale high-pressure die casting (HPDC) methods, such as gigacasting, which pioneered by Tesla, represent a major shift in production strategy, improving both efficiency and cost-effectiveness Tesla reported [4] a 40% cost reduction for the rear underbody of the Model Y by utilizing gigacasting, which replaced around 400 components with a single casting module. This approach also removed hundreds of robots from the assembly shop, then decreased production costs further. Following this trend, many automotive OEMs and suppliers are adopting similar technologies to integrate components, minimize welding and assembly operations, and significantly reduce cycle hours and production cost [5]. The cost reductions claimed by different companies were quite different, and it is hard to compare since they have different approach. However, there is no doubt that megacasting can save the cost significantly.

Megacasting also cuts energy requirements and lowers the overall carbon footprint. The process allows for the integration and replacement of around 100 components into a single part, significantly decreasing emissions from welding and logistics. In addition to efficiency gains, this method aligns with broader corporate sustainability and environmental responsibility goals.

Aluminum, especially as a lightweight structural material, plays a key role in enabling these benefits. It offers substantial weight reduction, improving fuel efficiency and reducing emissions during vehicle operation. However, producing primary aluminum is highly energy-intensive. Using recycled aluminum provides a more sustainable alternative, although it introduces technical challenges such as impurity control and consistency in alloy performance. Volvo reports that its megacasting project is helping the company achieve its sustainability goals of carbon neutrality by 2040, because it reduces the environmental footprint across production, allows for a high recycling content, and is made from a single alloy. The weight reduction, especially, since it replaced steel stampings, also helps to reduce the car's energy consumption during its use phase [6].

Despite these advantages, the increasing use of recycled aluminum also presents material sourcing challenges. The availability of clean, high-quality scrap suitable for structural applications remains limited, which may constrain large-scale adoption. At the same time, the scrap pool is expanding to include a broader range of trace elements such as iron (Fe), copper (Cu), and zinc (Zn), increasing the choices of raw materials. As a result, further research is needed to evaluate how these compositional variations affect mechanical behavior, defect formation, and casting integrity, particularly in demanding applications like megacasting.

1.2 Purpose

This thesis aims to investigate the mechanical performance and microstructural characteristics of secondary aluminum alloys used in megacasting applications. Mechanical performance is evaluated through tensile testing, three-point bending, and hardness testing. The focus is on understanding how varying levels of secondary aluminum content, particularly the presence of elements such as Fe, Cu, Zn, and V, influence mechanical behavior. The performance of these alloys is then compared to that of primary aluminum to assess any significant differences. Additionally, microstructural analysis, especially regarding intermetallic phases and shrinkages, is carried out to explore correlations between material performance and casting-related defects, with the goal of identifying whether such trends are primarily influenced by alloy composition or processing conditions.

The findings from this research aim to support broader implementation of secondary aluminum alloys in megacasting, contributing to sustainability objectives in the automotive industry.

1.3 Limitations

The thesis aims to finish in 20 weeks, therefore the scope of the project also requires clear limitations.

1. **The material tests we can take are based on the resource from Volvo Cars and Chalmers.**

The material tests will mainly be done at Volvo Cars considering the data security. External resource may be considered if some necessary tests cannot be done at the local company.

2. **The objectives are to increase the content of recycled aluminum in the megacasting, and to investigate how different element composition effect the mechanical performance and microstructure of the alloy.**
   Focusing the research and material testing on the combination of materials and the composition of different elements that are used in the megacasting. Increasing the use of secondary aluminum alloys means lower energy consumptions of producing raw material and lower carbon footprint. And looser requirements of the chemical composition means more choices in raw material selections.

2

Theory

This chapter summarizes the key theoretical concepts and literature necessary to understand the megacasting process and the use of secondary aluminum alloys.

2.1 Al-Si alloy

2.1.1 Al–Si phase diagram and microstructural formation

The Al–Si alloy system is a typical binary eutectic system, characterized by a eutectic point at approximately 12.6 wt.% Si and a temperature of 577 °C [7]. According to this phase diagram, alloys containing less than 12.6 wt.% silicon are classified as hypoeutectic alloys, wherein primary α-Al dendrites solidify first, followed by the formation of eutectic Al-Si. Conversely, hypereutectic alloys (>12.6 wt.% Si) first precipitate primary silicon particles before eutectic formation.

The Al–Si7 alloy investigated in this study is a hypoeutectic alloy, thus its microstructure typically comprises primary α-Al dendrites embedded in a eutectic mixture of α-Al and eutectic upon solidification.

2.1.2 Microstructural characteristics in Al-Si7 alloy

During megacasting, the rapid solidification typical of HPDC leads to significant microstructural refinement. The Al–Si7 alloy primarily consists of α-Al dendrites and eutectic, along with intermetallic phases and casting-related defects such as porosity and oxides.

The primary α-Al dendrites appear as bright, branched structures under microscopy. Their refinement enhances mechanical properties, particularly tensile strength and ductility. In unmodified conditions, eutectic typically forms coarse, needle-like or plate-like structures. However, chemical modification can transform these into finer, more rounded morphologies, significantly improving ductility and toughness.

Common intermetallic phases include α-Al(FeMn)Si and Chinese-script π-AlFeMgSi. The α-Al(FeMn)Si phase usually appears in a blocky morphology, in contrast to the needle-like β-AlFeSi phase, which is known to severely impair ductility and fracture resistance [8]. The addition of Mn promotes the transformation of the harmful β

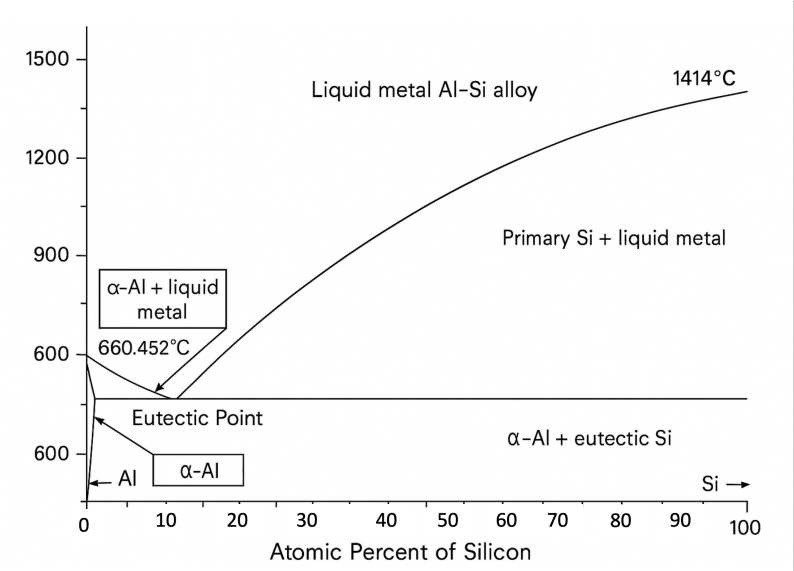

Figure 2.1: The Al-Si phase diagram

phase into the more benign α phase, while Cr can further stabilize it and improve thermal resistance. However, even the α-Al(FeMn)Si phase can negatively impact the balance between strength and ductility in Al–Si alloys [9].

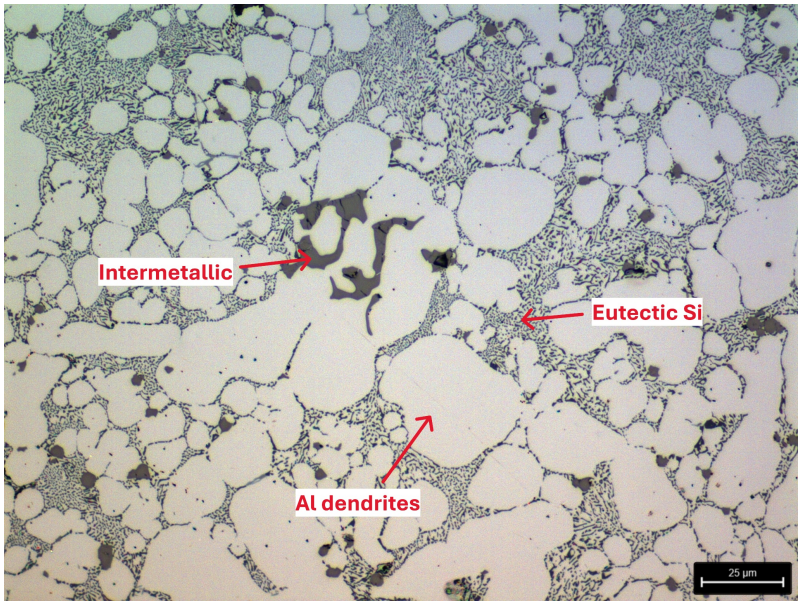

Figure 2.2: The morphology of α-Al dendrites, eutectic Si, and intermetallic

Casting defects such as oxides, gas porosity and shrinkage significantly degrade mechanical performance. Porosity usually forms due to gas precipitation or inadequate feeding during solidification, reducing tensile strength and elongation. Shrinkage porosity, caused by insufficient liquid metal compensation during cooling, similarly reduces mechanical reliability and fatigue resistance [10].

Morphologically, α-Al dendrites appear as coarse, tree-like structures and serve as

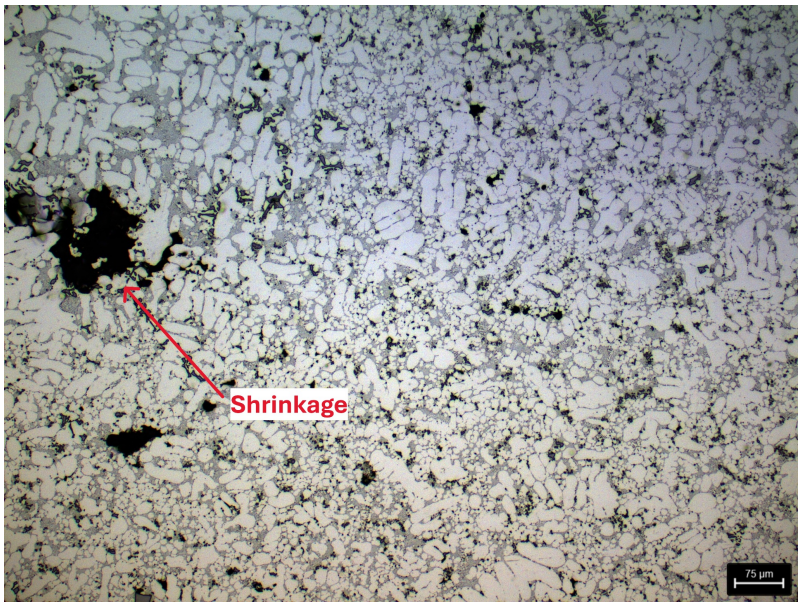

Figure 2.3: The morphology of a shrinkage pore

the backbone of the alloy's microstructure. Their size and morphology are influenced by cooling rate, alloy composition, and the presence of grain refiners, with slower cooling resulting in larger, less refined dendrites. Pre-solidification α-Al dendrites may also form during the Al-Si7 alloy casting process, potentially originating in the shot sleeve before full mold injection. These dendrites precipitate when the melt temperature falls below the liquidus line of the Al–Si phase diagram but remains above the eutectic point. They are still classified as primary α-Al dendrites, although they form earlier and outside the mold cavity.

A finer dendritic structure, typically achieved through rapid solidification processes like HPDC, contributes to higher tensile strength, better ductility, and improved fatigue resistance. In contrast, coarse and uneven dendrites can cause localized stress concentrations, promoting crack initiation and reducing mechanical integrity under tensile and bending loads. A refined dendritic network also enhances interdendritic feeding, reducing the occurrence of shrinkage and porosity. Therefore, optimizing the morphology of primary α-Al dendrites is essential for achieving a desirable balance between strength, ductility, and defect resistance in Al–Si alloys.

The cooling rate during solidification plays a key role in shaping the final microstructure of Al-Si7 alloys. Slow cooling rates tend to produce coarse α-Al dendrites, large eutectic plates, and coarse intermetallic compounds, which result in lower strength, reduced elongation, and diminished toughness. In contrast, rapid cooling—typical of HPDC and megacasting—leads to refined dendrites, finer eutectic, and smaller intermetallic phases. This microstructural refinement improves mechanical properties by minimizing stress concentration zones, delaying crack initiation, and enhancing both tensile and bending strength as well as overall toughness.

2.1.3 Effect of microstructural features on mechanical testing

A fine primary α-Al dendritic structure contributes significantly to enhanced mechanical properties, including ultimate tensile strength (UTS), yield strength (YS), and elongation. Unmodified eutectic tends to act as a stress concentrator, promoting early crack initiation and propagation, which reduces overall tensile performance. However, when modified with elements such as strontium (Sr), the eutectic becomes finer and more spheroidal, enabling more uniform stress distribution within the matrix and thereby improving tensile strength and ductility.

The presence of α-Al(FeMn)Si intermetallics generally has a negative effect on tensile properties, although the formation of π-AlFeMgSi phases can partially mitigate this by reducing embrittlement. Additionally, porosity and shrinkage defects significantly impair tensile performance. Gas porosity reduces the effective cross-sectional area, directly lowering UTS, YS, and elongation. Shrinkage cavities act as severe stress risers, leading to premature fracture and reduced mechanical performance.

In terms of bending behavior, fine α-Al dendrites and modified eutectic enhance ductility and toughness, improving overall bend performance. Conversely, coarse eutectic increases brittleness, leading to early fracture under bending loads. Porosity and shrinkage also compromise bending properties: gas porosity reduces structural continuity and causes localized stress concentration, while shrinkage cavities weaken the structure and lower resistance to repeated bending stress.

The β-AlFeSi phase is particularly harmful to mechanical performance. It typically forms as long, needle-like structures that act as severe stress concentrators, making the alloy vulnerable to crack initiation under load. These brittle, elongated intermetallics can significantly reduce both tensile strength and ductility by facilitating early fracture. Compared to the more compact and less harmful α-Al(FeMn)Si and π-AlFeMgSi phases, the β phase contributes more aggressively to embrittlement and is often associated with poor fracture toughness.

To minimize these effects, techniques such as vacuum-assisted casting, melt degassing, and optimized mold design—including improved gating systems, risers, and cooling channels—should be employed. These approaches improve interdendritic feeding and reduce defect formation, leading to enhanced hardness and overall mechanical performance of the casting.

2.2 Role of alloying elements in aluminum alloys

Aluminum alloys play a vital role in various industries due to their low density, high strength-to-weight ratio, and excellent corrosion resistance. However, pure aluminum is relatively soft and lacks the mechanical strength required for structural applications. To enhance its performance, alloying elements are added to improve strength, ductility, wear resistance, and thermal stability, making aluminum suitable for demanding environments. Common alloying elements include magnesium, sili-

con, copper, zinc, manganese, and vanadium, each of which modifies the microstructure and influences the alloy's mechanical behavior and environmental performance [11].

2.2.1 Silicon

Silicon (Si) is a key alloying element in HPDC aluminum alloys. It reduces shrinkage, improves castability, and enhances yield strength and ultimate tensile strength (UTS) [12]. Silicon forms an Al–Si eutectic network that contributes to higher strength, hardness, and wear resistance. Alloys containing 7–12 wt.% Si are common, as this range promotes the formation of fine eutectic structures, leading to improved mechanical properties. However, excessive silicon content can increase brittleness. The morphology of eutectic, particularly its size and shape—is a critical factor in determining mechanical performance. Fine, well-distributed eutectic enhances ductility, while coarse, plate-like structures act as stress concentrators and reduce ductility.

2.2.2 Magnesium

Magnesium (Mg) is a primary strengthening element in cast aluminum alloys, working Magnesium is a primary strengthening element in cast aluminum alloys and often works synergistically with copper. Higher Mg content enhances precipitation hardening, but it also promotes the formation of the π-AlFeMgSi intermetallic phase, an Fe-rich compound that can reduce ductility and embrittle the alloy [13]. To mitigate this, solution treatment is used to decompose the π phase, allowing more Mg and Si to dissolve into the aluminum matrix, which in turn enhances the aging response and mechanical properties [14].

Furui et al. reported that although magnesium has limited effect on peak isothermal hardness, increasing Mg content from 0.5% to 0.8% in Al–Si alloys significantly shortens the time required to reach peak hardness [15].

Magnesium also plays a critical role during the paint baking process used in automotive production, where it contributes to increased hardness and strength through natural or artificial aging.

2.2.3 Zinc

Zinc (Zn) is typically a minor alloying element in aluminum casting alloys, but it plays a significant role in high-strength applications, especially in aerospace and structural components. In the Al–Zn–Mg–Cu alloy system, Zn contributes to exceptional strength through precipitation hardening, making it one of the strongest aluminum alloy families. However, these alloys are also prone to stress corrosion cracking, which necessitates careful heat treatment and alloy design adjustments to improve long-term durability and resistance to environmental degradation [16].

2.2.4 Copper

Copper (Cu) is a key strengthening element in aluminum alloys, primarily through precipitation hardening. In Al–7Si–Mg alloys, adding 3–5% Cu has been shown to significantly improve tensile strength and fatigue resistance [17]–[20]. This makes Cu-containing aluminum alloys particularly well suited for aerospace and automotive applications where high mechanical performance is required [21], [22].

However, while Cu enhances strength, it also reduces corrosion resistance and ductility. Intermetallic phase as $AlCu_2$ can act as stress concentrators and promote brittle fracture. Regarding good corrosion resistance capability, additional protective measures, such as surface coatings or alloying with corrosion-resistant elements, are often necessary to ensure long-term durability in harsh environments [23].

2.2.5 Iron

Iron (Fe) is generally considered an impurity in aluminum alloys, but when properly controlled, it can contribute to increased strength and wear resistance. However, excessive iron leads to the formation of brittle intermetallic compounds, such as β-AlFeSi, which severely degrade ductility, toughness, and machinability.

Despite these drawbacks, iron has a positive effect on anti-soldering behavior in high-pressure die casting, making it beneficial in specific applications. To mitigate its harmful effects, controlling Fe content during alloy formulation is essential, ensuring a balance between mechanical performance and castability [24].

2.2.6 Manganese

Manganese (Mn) improves strain hardening and overall strength without compromising ductility or corrosion resistance. It is particularly beneficial in non-heat-treatable alloys, where it maintains mechanical performance through solid solution and dispersion strengthening [25]. Mn also contributes to grain refinement, enhancing toughness and reducing the tendency for hot cracking during welding.

Additionally, manganese improves workability, enabling aluminum alloys to be formed into complex shapes while retaining structural integrity [11]. It also reduces the harmful effects of excess iron by forming Fe–Mn intermetallic compounds, often referred to as “sludge particles”, which are less detrimental to ductility and mechanical stability than iron-rich β-phases.

2.2.7 Vanadium

Vanadium (V) is a less commonly used but valuable alloying element in aluminum alloys. It promotes grain refinement, leading to improved strength, toughness, and wear resistance. By reducing grain size, vanadium enhances fatigue performance and helps resist crack propagation under cyclic loading.

Vanadium also improves thermal stability, making it particularly suitable for high-

temperature applications such as aerospace structures and automotive engine components. However, due to its higher cost and specialized function, vanadium is not as widely used as other more common alloying elements.

2.2.8 Strontium

Strontium (Sr) is widely used as a modifier for eutectic in aluminum casting alloys. When added in small amounts, Sr transforms coarse, plate-like eutectic into fine, fibrous morphologies, which significantly enhances ductility, toughness, and fatigue resistance. With 50 to 250 ppm of Sr, eutectic grains nucleate more uniformly within the intergranular regions, resulting in a well-modified microstructure with improved mechanical behavior [26].

This refined morphology helps distribute stress more evenly, delaying crack initiation and propagation. As a result, aluminum alloys modified with strontium demonstrate superior impact toughness and mechanical reliability, particularly under dynamic or crash-load conditions.

2.3 Aluminum alloys usage in automotive industry

Numerous studies, especially from Research & Consulting [27], have shown that the use of aluminum in vehicles has steadily increased over the past decades, reaching over 180 kg per vehicle in Europe. Different types of aluminum alloys are used in various automotive components, depending on their required strength, formability, and other material properties.

Aluminum is the third most abundant element in the world, making up 8.23%, following oxygen at 46.10% and silicon at 28.20%. Since the automotive industry has begun to design vehicles that use less fuel and energy to reduce carbon footprint, aluminum alloys are one of the ideal materials that meet the demand for weight reduction with their characteristic properties such as high strength, good formability, excellent corrosion resistance and good potential in recycling [28].

Aluminum alloys are broadly categorized into wrought and casting alloys. Each group is designated by a four-digit code, indicating the main alloying elements and purity level. For wrought aluminum alloys, the first digit indicates the main alloying element or alloy group, while subsequent digits identify specific alloy compositions. For casting aluminum alloys, the designation similarly indicates the primary alloying elements and alloy composition, with a decimal point distinguishing cast forms. Examples of alloy designations and their interpretations are presented in Table 2.1.

Wrought aluminum alloys are produced through mechanical processes such as rolling, extrusion, or forging, which refine the grain structure and lead to enhanced mechanical properties and higher ductility. In contrast, cast aluminum alloys are made by pouring molten metal into molds, a process that is more cost-effective for complex

Alloy Type	Designation Series	Primary Alloying Element
Wrought Alloys	1xxx	≥99% Pure Aluminum
	2xxx	Copper (Cu)
	3xxx	Manganese (Mn)
	4xxx	Silicon (Si)
	5xxx	Magnesium (Mg)
	6xxx	Magnesium (Mg) and Silicon (Si)
	7xxx	Zinc (Zn)
	8xxx	Other elements (e.g., Li, Sn)
Casting Alloys	1xx.x	≥99% Pure Aluminum
	2xx.x	Copper (Cu)
	3xx.x	Silicon (Si) with Cu and/or Mg
	4xx.x	Silicon (Si) without Cu
	5xx.x	Magnesium (Mg)
	7xx.x	Zinc (Zn)

Table 2.1: Aluminum alloy designation system [29]

geometries but often results in higher porosity and lower ductility than wrought alloys [13].

One of the key distinctions between these two groups lies in their mechanical performance. Wrought alloys typically exhibit superior tensile strength and ductility due to grain refinement through plastic deformation. Cast alloys, while generally having lower mechanical strength, offer excellent corrosion and wear resistance. Wrought alloys can be strengthened through work hardening and heat treatment, whereas cast alloys are usually strengthened via alloying additions, such as silicon, copper, and magnesium [30].

The choice between wrought and cast alloys depends on the application. Wrought alloys are preferred for high-strength structural components, such as aircraft frames and performance-critical parts. Cast alloys are more suitable for engine blocks, transmission housings, and other components requiring complex shapes and good dimensional stability.

Consumers and manufacturers alike recognize the importance of vehicle lightweighting to reduce CO_2 emissions, but without sacrificing internal volume or payload. This makes body panel weight reduction particularly effective, prompting rapid development of aluminum sheets for external body components [31].

More automakers are shifting toward aluminum alloys to meet efficiency and environmental goals. While aluminum remains more expensive than traditional steel, it supports compliance with increasingly strict fuel economy and emissions regulations while maintaining structural performance and safety. Ongoing research continues to improve aluminum alloy formulations, making them even more suitable for modern automotive design. By 2030, the total aluminum usage per vehicle—including cast, extruded, and sheet products—is projected to reach approximately 256 kg per car

[32].

2.4 Key properties of a body structure part in automotive applications

The rear floor is a critical structural component located in the lower chassis area of a vehicle. It plays a vital role in supporting loads, protecting internal components, and distributing crash energy during collisions to ensure passenger safety. Therefore, manufacturing this part by a new method, such as megacasting, needs to focus on the following key properties to ensure vehicle safety.

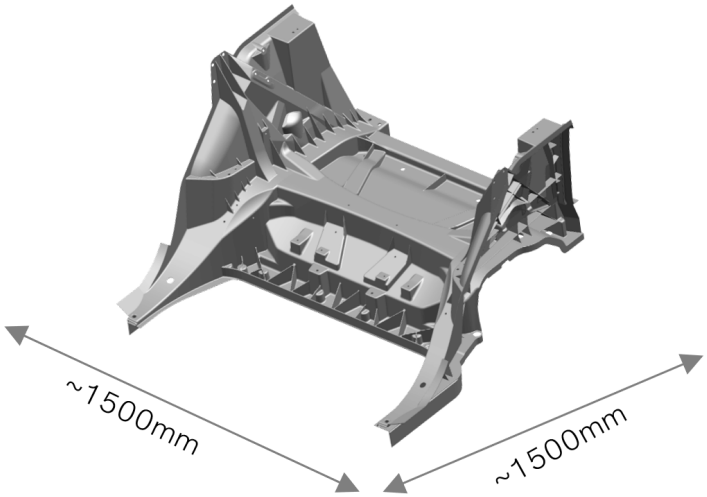

Figure 2.4: Early prototype design of a rear floor casting

2.4.1 Tensile yield strength, ultimate tensile strength & Young's modulus

Yield strength (YS) refers to the stress level at which a material begins to deform plastically, marking the point beyond which permanent deformation occurs. In the context of a vehicle's rear floor, this property is essential, as the component must support both static loads—such as the weight of passengers and cargo—and dynamic forces from road irregularities, vibrations, and driving maneuvers. A high yield strength ensures that the structure maintains alignment and functionality under these conditions, thereby preventing permanent distortion over the vehicle's operational lifespan.

Ultimate tensile strength (UTS), on the other hand, represents the maximum stress a material can withstand before fracturing. While yield strength governs performance under typical service conditions, UTS is critical during extreme events, such as collisions. In such scenarios, the rear floor must absorb and redistribute sudden

impact forces without fracturing. A high UTS enhances the crashworthiness of the vehicle and contributes directly to occupant protection by resisting catastrophic failure.

Young's modulus (E) describes the material's elastic stiffness, defining the ratio of stress to elastic strain in the linear region of the stress–strain curve. A high Young's modulus ensures minimal elastic deformation under load, helping the rear floor to maintain precise geometric stability and resist vibration or deflection that could impair fit or ride comfort.

Together, YS, UTS and Young's modulus provide a comprehensive picture of a material's load-bearing capacity. YS ensures long-term durability under daily use, UTS ensures safety and resilience under extraordinary conditions, and Young's modulus ensures that the component remains stiff and stable under elastic loads. These three properties are therefore fundamental to the design of structurally reliable and crash-resistant rear floor components in modern automotive applications.

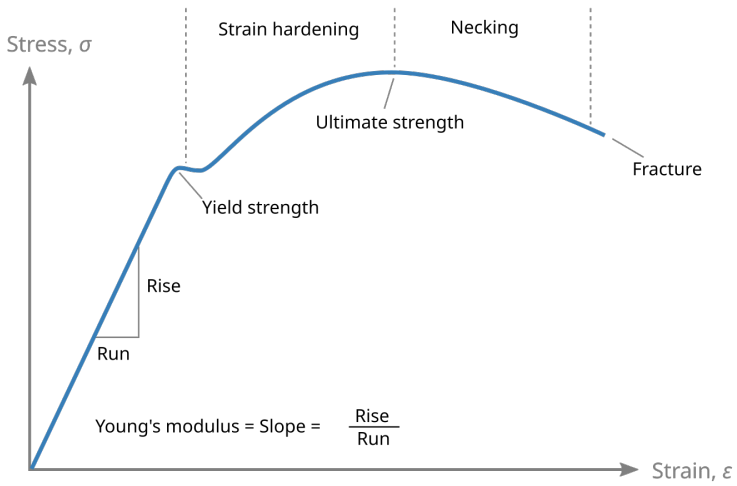

Figure 2.5: Stress-strain curve

2.4.2 Bend ductility

Bend ductility describes a material's ability to undergo plastic deformation during bending without cracking or fracturing. For the rear floor of a vehicle, this property is especially important due to the complex shapes and curvatures often required in its design. During manufacturing, the component must endure bending, shaping operations, and post-processing adjustments after high-pressure die castin , without developing surface cracks or internal defects. Insufficient bend ductility can lead to manufacturing defects or early-life failures, reducing overall structural integrity.

Beyond production, bend ductility plays a critical role in in-service performance. The rear floor is continuously subjected to torsional loads, uneven force distributions, and road-induced stresses—particularly under off-road or high-load conditions [33].

A material with high bend ductility can absorb and redistribute these loads without fracturing, helping maintain the vehicle's structural stability and passenger safety.

As such, bend ductility is a key parameter in achieving both manufacturability and operational durability, ensuring that the rear floor performs reliably across the vehicle's lifecycle.

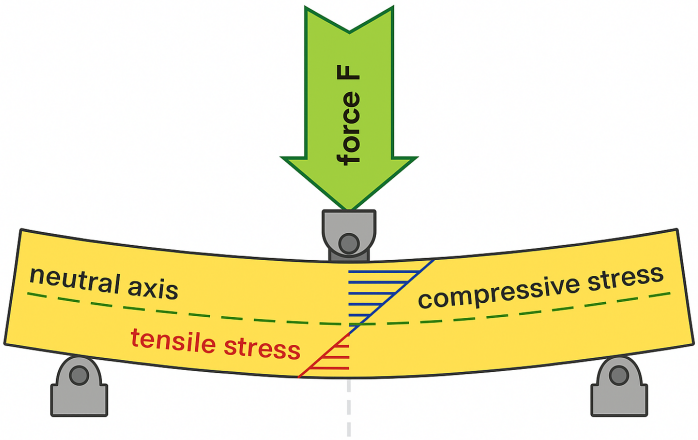

Figure 2.6: Distribution of bending moment

2.4.3 Hardness

Hardness measures a material's ability to resist deformation, indentation, or abrasion. For the rear floor, which is positioned on the underside of the vehicle, this property is particularly important due to frequent exposure to road debris, gravel, and other mechanical impacts. A higher hardness ensures that the surface remains intact under repeated contact, reducing the likelihood of dents, scratches, or surface fatigue that could compromise performance or appearance.

Hardness also contributes to durability by improving resistance to wear and localized damage, extending the service life of the component. For example, structual HPDC alloys with Brinell hardness values ranging from 80 to 120 HB are commonly used in automotive structural applications, offering a balance between wear resistance and ease of manufacturing [34].

By preserving surface integrity, a high level of hardness reduces the need for frequent maintenance or replacement, ultimately enhancing the vehicle's reliability and cost-effectiveness over time.

2.4.4 Fatigue resistance

Fatigue resistance refers to a material's ability to withstand repeated cyclic loading without developing cracks or failing over time. This property is especially critical for the body structure of a vehicle, which is continuously exposed to dynamic forces such

as road vibrations, engine oscillations, and shifting loads from passengers or cargo. These forces create millions of stress cycles throughout the vehicle's operational life, making fatigue resistance essential for long-term reliability.

Fatigue failures often initiate at stress concentrators, such as inner corners, edges, or welded joints, where localized stresses exceed the material's fatigue limit. In rear floor applications, adequate fatigue resistance helps prevent crack formation and propagation, preserving the integrity of the component under both normal and extreme driving conditions.

High fatigue resistance also supports lightweighting strategies, allowing for thinner structural sections without sacrificing performance. By ensuring that these thinner parts still meet durability requirements, fatigue-resistant materials contribute to more efficient and sustainable vehicle designs.

2.4.5 Corrosion resistance

Corrosion resistance describes a material's ability to withstand chemical or electrochemical reactions caused by environmental exposure, such as moisture, salts, and pollutants. This property is essential for the rear floor, which is part of the vehicle's underbody and frequently exposed to road salt, rainwater, mud, and debris. Without adequate corrosion resistance, materials can deteriorate over time, leading to reduced structural integrity, safety risks, and increased maintenance costs.

Aluminum alloys commonly used in automotive applications form a protective aluminum oxide layer on their surface, which naturally resists corrosion. In addition, OEMs often apply protective coatings or paint layers to further shield the material from aggressive environments. However, impurities, casting defects, or mechanical damage can disrupt this passivation layer, making the material susceptible to localized corrosion such as pitting.

Modern aluminum alloys are engineered with low impurity levels and optimized alloying elements to enhance corrosion performance [35]. Ensuring high corrosion resistance not only extends the component's service life but also contributes to the overall sustainability and long-term reliability of the vehicle, particularly in regions with harsh weather or heavy road salt usage.

Due to limitations in experimental resources, testing time, and sample availability, this thesis focuses on evaluating the materials' yield strength, ultimate tensile strength (UTS), bend ductility, and hardness. The assessment of fatigue and corrosion resistance will be conducted separately by other research colleagues, and their results will be used to complement the findings of this study.

2.5 Challenges in using recycled aluminum for structural castings

From both a cost-efficiency and sustainability perspective, aluminum is one of the most economical and strategically valuable materials in automotive manufacturing. With increasing pressure on the industry to achieve carbon neutrality and environmental responsibility, manufacturers are transitioning toward lightweight materials such as aluminum to reduce emissions and energy consumption. Traditionally, body structures have been produced using steel, valued for its mechanical strength and low cost. However, cast aluminum has gained prominence in recent years due to its excellent machinability, formability, and corrosion resistance [36]. With a density roughly one-third that of steel, aluminum can offer substantial weight reduction, contributing directly to improved fuel economy and reduced CO_2 emissions [37].

Despite these advantages, the primary production of aluminum—particularly through bauxite mining and electrolysis—is extremely energy-intensive. The process begins with extracting alumina from bauxite using the Bayer process, after which it is refined into primary aluminum through electrolytic reduction. This transformation consumes a considerable amount of electricity, with a rough ratio of 2 tons of alumina required to produce 1 ton of aluminum [38].

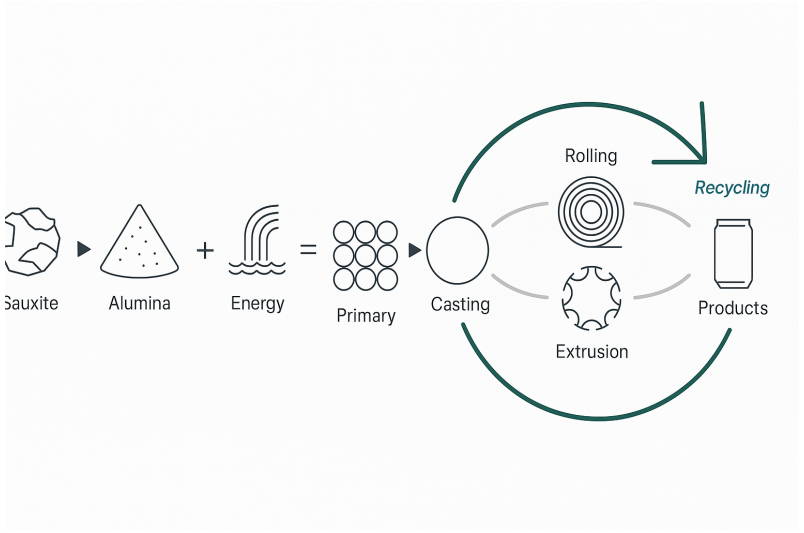

Figure 2.7: Illustration of the aluminum life cycle

Modaresi and Müller developed a dynamic model to assess aluminum flows in automobiles worldwide, estimating that up to 56% of the mass of cast alloys could be composed of scrap (assuming 70% of cast alloys are secondary, and these contain up to 95% recycled content) [39]. This finding highlights the immense potential for energy and emissions savings, as producing secondary aluminum requires only about 5% of the energy needed for primary production [40].

Unlike many materials, aluminum can be recycled indefinitely without degrading its core properties, making it uniquely valuable in the circular economy. In the

automotive sector, scrap aluminum retains high market value. According to the International Aluminium Institute [41], producing 1 ton of primary aluminum requires around 14 MWh of electricity, generating up to 12 tons of CO_2 emissions, and compared with steel, it can emit over 1.2 tons during production.

Although recycling aluminum requires only a small fraction of the energy needed for primary production, it often introduces elevated levels of impurities and residual alloying elements, which can compromise mechanical properties. Scrap aluminum frequently contains trace amounts of iron (Fe), silicon (Si), copper (Cu), zinc (Zn), and other elements from previous applications. These contaminants can lead to increased porosity, reduced ductility, and lower overall performance in structural components [42].

To address this, several strategies have been explored in the industry. One approach is to dilute secondary aluminum with primary aluminum, thereby lowering impurity levels. While this method can be effective in meeting compositional requirements, it limits the potential to maximize recycled content. Another strategy involves downcycling, where recycled alloys with higher contamination are used in less demanding applications. However, this often results in economic inefficiencies and reduces the long-term value of recycled material [43].

A more technically robust solution lies in advanced refining and filtration techniques. As highlighted by Padamata, the aluminum recovery process typically includes both physical separation and chemical refining [44]. Physical separation methods—such as magnetic separation, air classification, eddy current sorting, sink-float separation, and color sorting—are used to remove unwanted inclusions based on material properties. These are then followed by refining processes, including the Hoopes process, flux treatments, and gas fluxing, which serve to remove dissolved impurities and improve alloy purity. Among these options, filtration and refining are considered the most critical for enabling high-performance applications using secondary aluminum.

Aluminum scrap availability is increasing globally, driven by rising consumption across industries such as transportation, construction, and packaging. One of aluminum's unique advantages is that it can be recycled indefinitely without degrading its inherent properties, making it a cornerstone material in the circular economy. According to the International Aluminium Institute (IAI), more than 75% of all aluminum ever produced is still in use today, underscoring its long-term value and sustainability potential [41].

The automotive industry is a major contributor to scrap aluminum generation. End-of-life vehicles (ELVs) serve as a rich source of recyclable material, while production scrap—generated during stamping, trimming, and machining—offers a consistent stream of high-quality, clean aluminum. This supply is expected to grow further with the increased adoption of lightweight vehicle designs and electric vehicles (EVs), both of which require greater aluminum content per unit compared to traditional internal combustion engine vehicles.

Market forecasts suggest that the demand for secondary aluminum will outpace that of primary aluminum in the coming decades. According to Spherical Insights, the recycled aluminum market is expected to grow at a compound annual growth rate (CAGR) of 8.16% between 2021 and 2030, rising from USD 5.6 billion to USD 25.12 billion [45]. Europe and North America, supported by well-established recycling infrastructures, are projected to lead this transition, while emerging economies are rapidly investing in scrap collection and processing technologies to follow suit.

In summary, the outlook for aluminum scrap availability is highly promising, offering tremendous potential to reduce energy consumption and carbon emissions in aluminum production. However, the key to unlocking this potential lies in maintaining alloy quality through better scrap management, advanced refining methods, and thoughtful alloy design. These elements are essential for expanding the use of recycled aluminum in demanding applications such as megacasting for automotive structures.

2.6 High-pressure die casting

High-pressure die casting (HPDC) is a mature and widely adopted metal forming technology. It was developed over a century ago and was originally used primarily for zinc [46]. Today, HPDC is well suited for high-volume production and is employed in various industries, with approximately 50% of global light metal castings produced using this method [47]. Until the late 1990s, HPDC was typically used for simple castings with secondary alloys and was not regarded as a sophisticated manufacturing technique. However, as the automotive industry evolved and new vehicle models demanded more complex parts, engineers advanced HPDC into a higher-quality process that enabled heat treatment, welding, and improved ductility and strength.

A simultaneous trend in casting is the push for larger components with reduced weight, which requires lower wall thickness and more complex geometry. The complexity of a part is determined by its weight, size, geometry, and ability to resist deformation [46]. As a result, HPDC is now capable of producing complex automotive components that meet modern structural requirements.

Megacasting is an evolution of HPDC that enables the casting of large aluminum components, such as entire vehicle underbodies. It follows the same HPDC principles but at an unprecedented scale, requiring massive die-casting machines—often with more than 6,000 tons of clamping force—and advanced control over material flow and thermal behavior.

When aluminum is used as the raw material, cold-chamber die casting machines are typically employed. In this setup, the metal injection system only comes into contact with molten aluminum for a short period. A furnace maintains the molten metal at a stable temperature before transferring it to the shot sleeve for each cycle. The HPDC process involves multiple steps, including die lubrication and cooling,

mold closing and opening, and metal injection.

The main steps of the HPDC production process are shown in Figure 2.8.

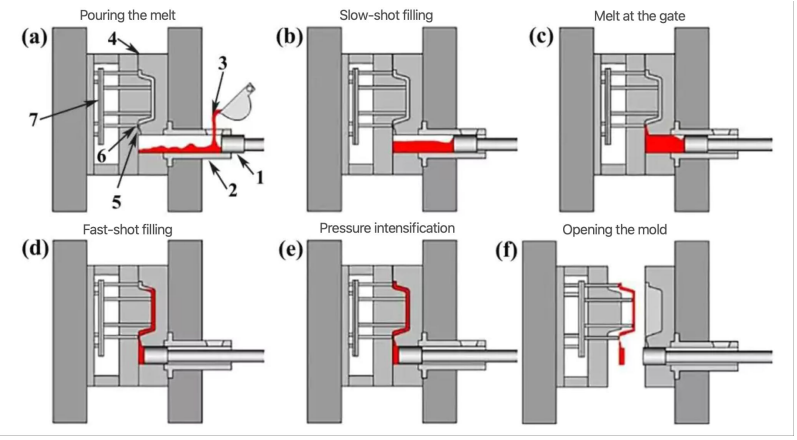

Figure 2.8: The general process of HPDC

2.6.1 Mold and die preparation

The HPDC process begins with the design and fabrication of large-scale molds and dies. These components must be engineered with high precision and durability to withstand extreme temperatures and pressures. The dies are typically made from high-grade tool steel and are coated with specialized materials to extend their service life and withstand the repeated high-pressure injection of molten aluminum. Integrated cooling channels are designed into the dies to regulate temperature and promote uniform solidification.

2.6.2 Molten aluminum preparation and injection

Once the mold is properly prepared, molten aluminum is injected into the cavity. The molten aluminum must be kept at the optimal temperature, typically around 660–720 °C, to maintain fluidity while minimizing oxidation. Before injection, the molten metal is treated using degassing and filtration techniques to eliminate impurities and enhance the final casting quality [48].

The injection process in HPDC typically consists of three phases. In the initial phase, the plunger moves slowly through the shot sleeve to avoid air entrapment. During this stage, cavity pressure remains low. In the second phase, the plunger velocity gradually increases, and the refined molten aluminum is injected rapidly into the mold cavity at high speed and pressure, with metal velocities reaching 30–60 m/s [49], [50]. This ensures the mold cavity is completely filled within a short time, forming detailed features while minimizing porosity. The cavity pressure begins to rise as filling progresses. In the final phase, injection pressure can reach 200–400 bar, which is crucial to ensure complete filling and enhance structural integrity of large-scale components. This step is especially important for reducing shrinkage porosity and improving the mechanical properties of the casting. Given the large

size of megacast parts, precise control of thermal gradients and solidification rates is essential to prevent warping and internal defects [48].

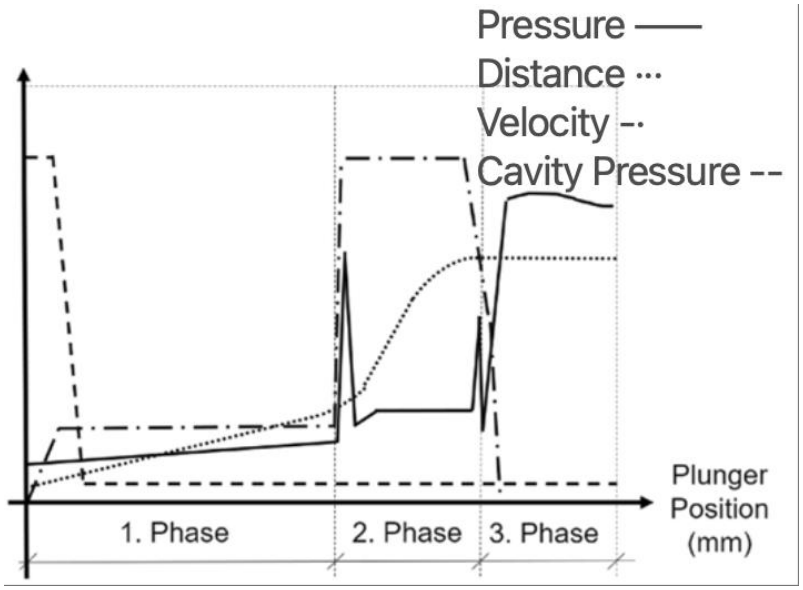

Figure 2.9: Three phases of the shot curve in HPDC

2.6.3 Solidification, cooling and ejection

After injection, the molten aluminum begins to solidify within the mold. The cooling process must be precisely controlled to minimize thermal stresses and reduce the formation of shrinkage defects. Vacuum-assisted casting is often employed to decrease gas porosity and improve the mechanical performance of the casting. Additionally, multi-zone cooling systems integrated into the die help maintain uniform temperature distribution, resulting in more consistent mechanical properties throughout the component.

Immediately after the part is ejected from the mold, water quenching is applied to accelerate solidification. This rapid cooling creates a finer microstructure and helps suppress the formation of coarse intermetallic phases, thereby enhancing mechanical strength—particularly in heat-treatable alloys. However, quenching must be carefully timed and controlled to avoid distortion and residual stresses caused by uneven temperature gradients.

Once solidification is complete, the casting is ejected from the mold. Most molds are equipped with ejector pins that automatically release the casting, ensuring a smooth and efficient transition to subsequent processing steps [51].

2.6.4 Trimming, deburring, and surface machining

After casting, excess material—including flash and feeder residues—must be removed through trimming and deburring. These processes involve robotic cutting,

laser trimming, and CNC milling, which ensure the component meets precise dimensional and surface finish requirements. Machining is also required to create critical features such as mounting points, threaded holes, and fine tolerances that cannot be achieved during casting alone.

To improve precision and consistency, automated robotic arms equipped with milling tools are commonly used, reducing the need for manual labor and increasing production efficiency [48]. This step is essential to meet the stringent specifications of structural automotive components and to prepare the casting for any subsequent surface treatment or assembly.

2.6.5 Heat treatment and strengthening

Heat treatment is a critical step in the HPDC process, as it enhances the mechanical properties of aluminum alloys by improving strength, ductility, and fatigue resistance. Without proper heat treatment, components may lack the structural integrity required for demanding applications such as automotive body frames.

Here are several ways of heat treatment introduced in Figure 2.10, each of them can achieve specific mechanical properties.

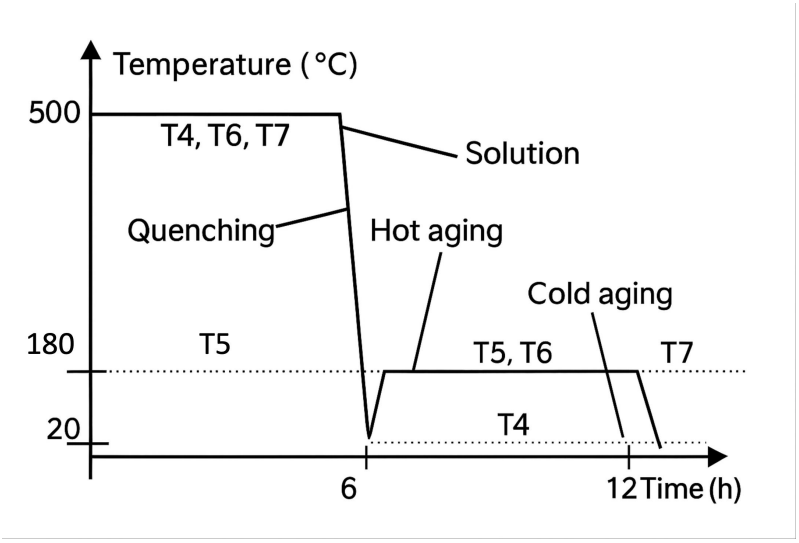

Figure 2.10: Different ways of heat treatment

The most common method for aluminum components is T6 treatment and T7 for body parts. The aluminum casting is first heated at a very high temperature, typically 480-540 °C for about 6 hours by solution annealing. Solution heating can fully dissolve alloying elements into the aluminum matrix to form a supersaturated solid solution, and it is critical for distortion of large and thin castings. Then the casting need to be rapidly quenched in a water or other liquid at a temperature to lock the solution annealed structure. The quenching process often causes distortion and stresses in parts. This is because of the extreme temperature differentials between the heated casting and the quench cooling solution.

The casting is finally hot aged in a furnace, where it is heated to around 180 °C for about 6 hours. For T6, natural cooling follows this stage, resulting in a harder aluminum with improved resistance to deformation under high loads [52]. In contrast, the T7 treatment uses extended aging and slower cooling, a process known as over-aging, which produces a more dimensionally stable material with lower strength. In some cases, a straightening process is required after quenching to restore dimensional accuracy.

Another approach is T5, which is also an artificial heat treatment aging process. It usually carried out at temperatures between 150-200 °C. The slower thermal exposure, usually around 12 hours, stabilizes the microstructure and relieves residual stress. While T5-treated components do not achieve the same strength as those treated with T6, they exhibit less distortion and are often easier to machine [53].

Due to cost, cycle time and sustainablity reasons the megacasting parts are preferably not heat treated. The body paint process in automotive manufacturing involves a series of heating steps that can indirectly act similar to a T5 heat treatment for aluminum components. After casting, the aluminum parts typically go through cleaning and pre-treatment before entering the paint shop. The key steps include the electrodeposition coating baking, primer baking, middle and top coating baking. Each of these steps involves heating the car body to high temperatures. For instance, the body is typically held at 170-180 °C for around half an hour. Then primer baking often follows at 160-180 °C for around half an hour, and finally, top coating baking is done at 140-160 °C for another half an hour. These successive thermal cycles help artificially age the aluminum alloy, leading to precipitation hardening without a separate artificial aging process. This process simulates the T5 heat treatment, enhancing the mechanical properties of the aluminum components without requiring a standalone heat treatment line.

2.6.6 Inspection and quality control

Due to the high complexity and structural importance of megacasting components, rigorous inspection is required to ensure quality and performance. X-ray scanning is commonly used to detect internal defects, such as porosity, cracks, or inclusions, which may compromise structural integrity. Dimensional accuracy is verified using laser scanning and digital twin simulations, comparing the physical casting with the CAD model to identify deviations.

For surface quality control, visual inspection is typically employed, often supported by high-resolution imaging systems for defect detection.

In addition to non-destructive testing, manufacturers also perform mechanical testing such as tensile and fatigue tests to ensure that the parts meet crashworthiness and durability standards. Components that fail to meet specifications of visual inspection and NDT are either scrapped for recycling or sent for rework machining to salvage usable sections.

2.7 The snake tool - R&D test component

The snake tool is a specialized die-casting mold designed to evaluate the castability of aluminum alloys and the impact of process modifications, particularly in high-pressure die casting (HPDC). Featuring narrow, intricate channels and complex geometries including flat and beam structures, the snake tool challenges the flow behavior of molten metal, helping engineers assess whether it can completely fill the mold without developing defects such as cold shuts, porosity, or incomplete sections.

Serving as a scaled-down surrogate for megacasting dies, the snake tool offers significant advantages in material and time savings during early-stage experimentation. Its compact form makes it ideal for testing recycled alloys, especially when investigating how variations in chemical composition and impurity content affect castability and final part quality.

The tool includes features such as a squeeze pin, jet cooling system for all precast holes, a vacuum-prepared full-length shot sleeve, and plunger tips. The die casting machine (DCM) typically operates in the 1000–2000 ton range, with a target cycle time of 80 seconds. This setup enables the evaluation of how different process parameters and alloy selections correlate with performance, such as defect formation, structural integrity, and flow uniformity.

Using the snake tool, it becomes possible to optimize parameters like alloy composition, mold temperature, injection speed, and gating system design. By observing how the molten metal behaves within the complex geometry, engineers can identify flow deficiencies and defect-prone regions, providing crucial insights before moving to full-scale production.

This approach minimizes material waste, reduces trial-and-error iterations in full-scale casting, and supports early-stage validation of structural integrity. It is particularly effective when working with recycled aluminum alloys, where variability in composition and inclusion content may lead to unpredictable casting behavior.

However, testing on the snake tool captures the combined influence of both casting conditions and raw material characteristics. As a result, distinguishing between defects caused by process parameters and those stemming from alloy composition becomes essential. Accurate interpretation of these combined effects is critical for identifying the root causes of performance variation and for developing robust, recyclable-friendly casting strategies.

Figure 2.11: The design of snake tool

2.8 Cast trail

2.8.1 Process parameter

The casting trials were carried out using a high-pressure die casting (HPDC) machine with a clamping force between 1000 and 2000 tons closely mirroring the pressures and speeds used in full-scale industrial settings. The process was fine-tuned to run on an 80 second cycle, striking a balance between efficient production and ensuring proper cooling and part quality.

Sl.no	parameter	value
1	Die casting machine	1000-2000 ton clamping force
2	Cycle time	80 seconds
3	Melt temperature	680°C ± 5°C
4	Holding furnace temperature	690°C

Table 2.2: Process parameter

2.8.2 Alloy composition table

Sl.no	Batch		Parts
1	Standard (Primary)	A4	6
2	High recycle content (Internally recycled)	B1	3
3	High recycle content Fe 0.3%	B2	2
4	High recycle content Fe 0.5% + V 0.2%	B3	1
Total			**12 snakes**

Table 2.3: Alloy Table

2.8.3 Challenges during the trails

Despite the controlled setup, multiple challenges were encountered.

Porosity and Entrapment Defects: During the initial casting runs, the presence of centerline porosity and surface blisters was observed in several components. These defects were primarily attributed to inadequate vacuum draw and the entrapment of air within the narrow channels of the SnakeTool. The trapped air formed voids during solidification, resulting in both internal porosity and external surface irregularities.

Die Temperature Instability: Another significant issue encountered during the initial stages of the casting trials was the inconsistency in die temperature, particularly during the early shots of each cycle. This thermal imbalance resulted in incomplete mold filling, as well as uneven surface finishes on the cast components. Such non-uniform temperature distribution across the die negatively affected the fluidity of the molten metal and the solidification pattern, increasing the risk of cold shuts and surface defects.

Process vs Material Effects: One of the more intricate challenges encountered during the casting trials was figuring out whether certain defects were due to process settings or the alloy composition itself. For example, shrinkage porosity could be traced back to either low intensification pressure or the presence of certain elements in the alloy, like high levels of iron or silicon.

3

Methods

3.1 Material selection and sample preparation

The goal of this study is to analyze the fundamental differences among primary and secondary aluminum alloys, and aluminum alloys with different chemistry composition produced via High-Pressure Die Casting (HPDC), with a focus on their mechanical properties and structural performance. The materials investigated include standard primary aluminum (A4), used as a baseline reference, internally recycled aluminum alloys with the same composition (B1), and materials that have been compositionally modified with elevated levels of iron (Fe), copper (Cu), and zinc (Zn), specifically Fe 0.3% (B2), and Fe 0.5% combined with V 0.2% (B3).

Sl.no	Batch	Parts
1	A4	6
2	B1	3
3	B2	2
4	B3	1
Total		**12 snakes**

Table 3.1: Alloy Table

The samples are produced using the High-Pressure Die Casting (HPDC) process with the snake tool, which allows for strict control of critical process parameters to ensure consistent casting quality. Injection speed and pressure are precisely adjusted to achieve uniform mold filling and minimize porosity, while the melt temperature is maintained at a stable level to support optimal microstructural development.

After casting, the parts undergo a series of post-processing operations. The first step is quenching, during which the samples are rapidly cooled to preserve the microstructure and enhance mechanical properties. This is followed by trimming, where excess material is removed. The parts are then cut into specific dimensions according to the requirements of subsequent mechanical tests. At this stage, the samples are prepared for the paint body cycle, a controlled thermal treatment designed to modify surface properties as an artificially age hardening and simulate industrial paint-curing conditions.

Following the thermal treatment, each sample is systematically labeled and sectioned in accordance with VDA and ISO standards, indicating whether it is intended for tensile or three-point bending tests. The samples are then machined to precise dimensions and tolerances to meet testing requirements. Surface preparation—including grinding and polishing—is performed to eliminate surface imperfections and enable accurate microstructural analysis. Consistent labeling and documentation are maintained to ensure a well-organized dataset and efficient data tracking throughout the study.

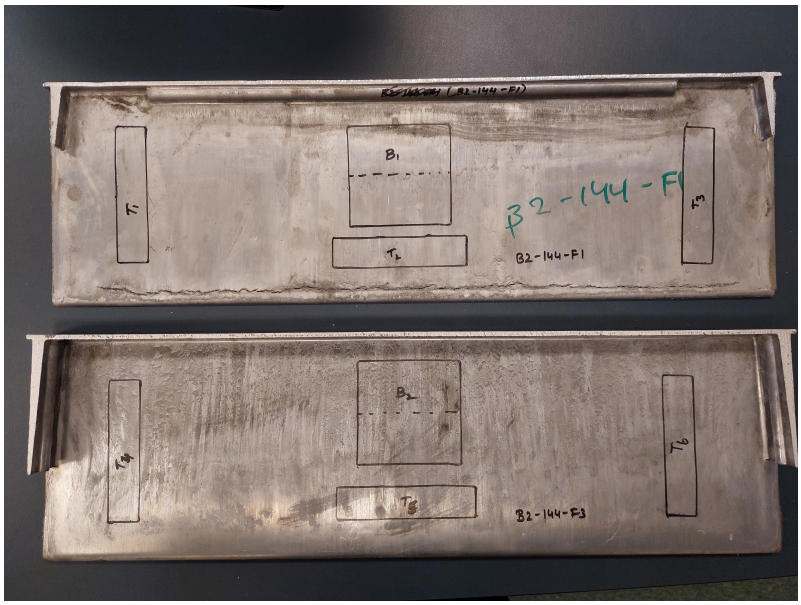

Figure 3.1: Samples marked for cutting

3.2 Mechanical testing methods

For mechanical testing, each sample was machined to precise dimensions in accordance with VDA and ISO standards. To ensure the accuracy of microstructural evaluations, all specimens underwent grinding and polishing to eliminate surface imperfections. In addition, each sample was systematically labeled and recorded to ensure traceability and consistency in data collection.

3.2.1 Tensile testing

Tensile testing was performed in accordance with ISO 6892, with six samples taken from each part—three from the front plate (F1) and three from the rear plate (F3)—resulting in a total of 72 specimens. The sample distribution includes 36 samples from the primary composition (A4), 18 from the secondary composition (B1), 12 from the Fe 0.3% batch (B2), and 6 from the Fe 0.5% + V 0.2% batch (B3). Each specimen was 85 mm in length, with a 10 mm gauge width, 15 mm wide ends, and 3 mm thickness. The test was used to determine yield strength, ultimate tensile strength (UTS), and elongation.

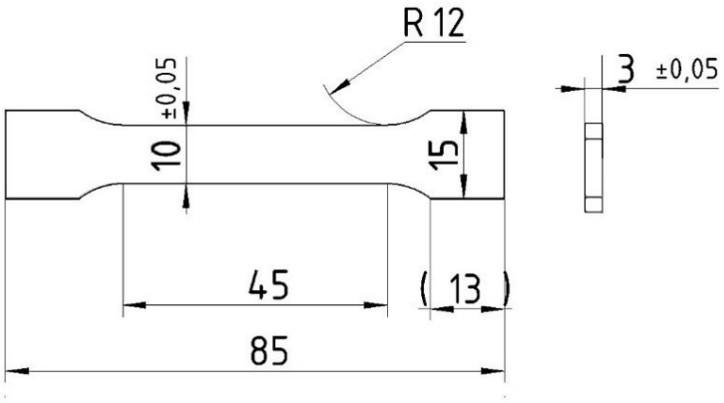

Figure 3.2: Tensile sample geometry

Sl.no	Batch	Parts	Samples
1	A4	6	6*6=36
2	B1	3	3*6=18
3	B2	2	2*6=12
4	B3	1	1*6=6
Total		**12 snakes**	**72 samples**

Table 3.2: Tensile test samples

3.2.2 Bending testing

The three-point bending test was conducted according to VDA 238-100 standards, with each specimen having dimensions of 60 mm × 60 mm. A total of 24 samples were tested—two from each batch, including one from F1 and one from F3. The bending samples were labeled as B1 and B2, corresponding to their respective positions within the casting. The testing parameters and sample information are summarized in Table 3.3.

Parameter	Value
Specimen Length	60 mm
Specimen Width	60 mm
Specimen Thickness (t)	3 ± 0.15 mm
Support Span (L)	$2t$ (twice the thickness)
Roller Radius	15 mm
Punch Radius	0.4 mm
Punch Angle	90°
Test Speed (Crosshead Speed)	10 ± 2 mm/min

Table 3.3: Parameters for three-point bending test

Sl.no	Batch	Parts	Samples
1	A4	6	6*2=12
2	B1	3	3*2=6
3	B2	2	2*2=4
4	B3	1	1*2=2
Total		**12 snakes**	**72 samples**

Table 3.4: Bend plate test sample

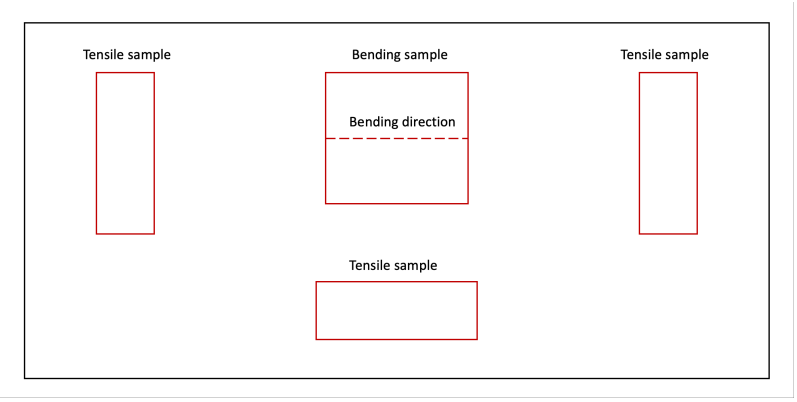

Figure 3.3: 3-point bending sample direction

3.2.3 Hardness testing

Brinell hardness testing was performed on a selection of 10 samples, comprising 5 from F1 and 5 from F3. Each sample received four indentations arranged in a zig-zag pattern, resulting in a total of 40 indentations across all specimens. This approach allowed for a representative assessment of surface hardness variation across different casting positions.

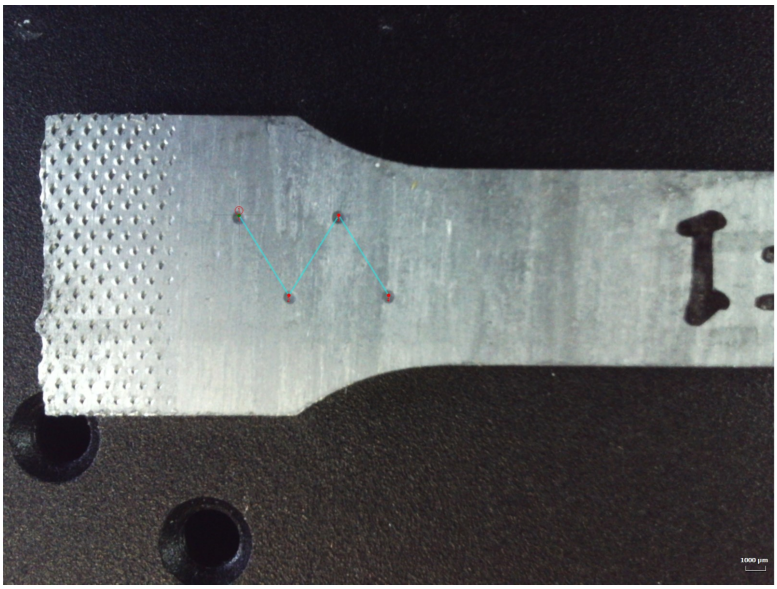

Figure 3.4: Hardness test zig-zag pattern

Sl.no	Flat	Samples
1	F1	5
2	F3	5
Total		**10 samples**

Table 3.5: Hardness test sample

These tests provide valuable insights into chemistry compositions and processing parameters influence mechanical performance.

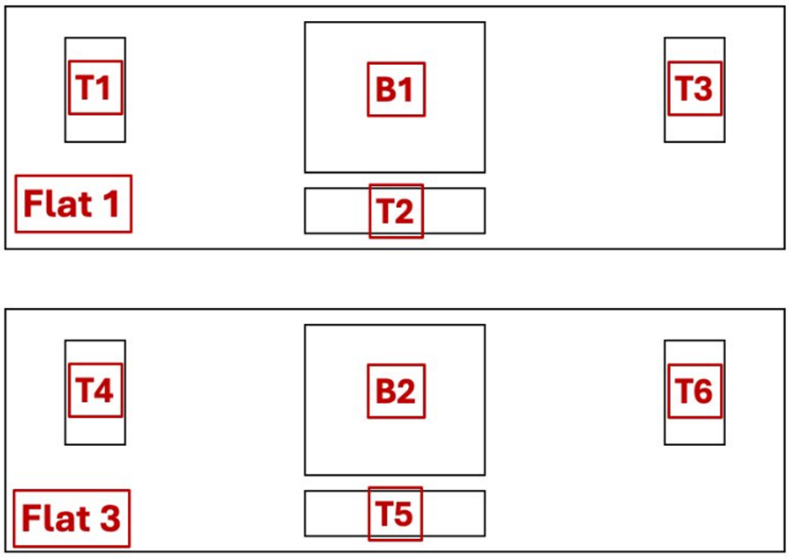

Figure 3.5: Test samples indication

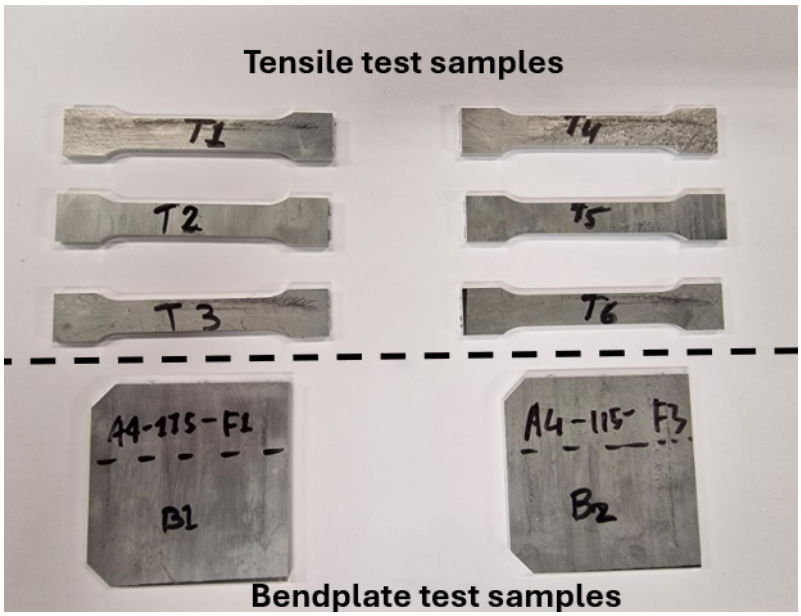

Figure 3.6: Test samples

3.3 Microstructural analysis

3.3.1 Optical microscopy

After the tensile tests were completed, a subset of samples was selected for further optical microscopy analysis based on notable mechanical performance or distinctive fracture characteristics. To ensure consistency and enable comparative evaluation across all alloy batches, one specimen was selected from both F1 and F3 in each of the four batches (A4, B1, B2, and B3).

This sampling approach provided a balanced representation of material and positional variation. Observing these specimens under the microscope enabled the identification of surface-level differences and trends related to porosity, shrinkage, and casting defects. These features are critical for understanding how variations in recycled content and elemental composition affect the material's behavior.

While optical microscopy provides only a preliminary impression of microstructural and fracture characteristics, it offers valuable insight into the overall fracture mode and porosity distribution. However, for more detailed and quantitative microstructural analysis, further investigation through metallography and fractography is necessary.

3.3.2 Metallography

Proper metallographic preparation is critical for reliable microstructural evaluation, with grinding and polishing being particularly important. The ideal surface condition is scratch-free, allowing for clear and accurate observation. Each sample was mounted, ground, and polished to produce metallographic specimens, which were

then examined under an optical microscope to assess microstructural features.

A total of eight samples were selected, one from F1 and one from F3 for each of the four batches. This selection strategy ensured a comprehensive comparison across both material compositions and casting positions. The samples were extracted from the gauge section of the fractured tensile specimens, providing insight into how the material behaved under mechanical stress.

The preparation process followed standard metallographic protocols, beginning with mounting and progressing through sequential grinding with silicon carbide papers, from P240 to P4000 grit. After polishing, the samples were examined under a Leica optical microscope at magnifications ranging from 50× to 250×. The focus was placed on identifying and characterizing features such as shrinkage cavities, porosity, intermetallic phases, and grain size, all of which significantly influence mechanical performance.

To assess manufacturing quality, metallographic images were compared across batches and positions, with particular attention paid to shrinkage severity. The software Fiji ImageJ was employed to quantify shrinkage by calculating the area fraction of shrinkage features in each image. Fiji is an open-source image processing software widely used for quantitative analysis of scientific images. Built on the ImageJ platform developed by the NIH, it supports tasks such as image enhancement, measurement, threshold segmentation, and region-based analysis. In the field of materials science, Fiji is particularly well suited for the processing and analysis of metallographic images, enabling quantitative evaluation of parameters such as porosity, shrinkage area ratio, particle size, and morphology.

3.3.3 SEM

To gain a more detailed understanding of the microstructure and better observe the influence of recycled content on alloy behavior, Scanning Electron Microscopy (SEM) was employed. This technique provides high-resolution imaging, enabling the visualization of key features such as intermetallic particles, grain boundaries, and other microstructural characteristics.

The SEM analysis was performed on the same eight samples previously examined using optical microscopy, one from F1 and one from F3 in each of the four batches. Special emphasis was placed on evaluating intermetallic phases, which are known to negatively affect ductility and fracture resistance. Therefore, the size, morphology, and quantity of intermetallics were the primary focus of this section.

Prior to imaging, all samples were coated with a thin layer of silver to minimize surface charging during electron beam exposure and to enhance image clarity. The SEM was operated in backscattered electron (BSE) mode, which enhances contrast between different phases within the alloy. Images were captured at magnifications ranging from 500× to 5000×, depending on the level of detail required for observing intermetallic particle size, shape, distribution, and density.

3.3.4 X-ray

X-ray inspection was conducted on all samples to identify internal defects, including cracks, shrinkage porosity, and inclusions, across three batches (A4, B1, and B2) and casting positions (F1 and F3).

This non-destructive evaluation (NDE) method allowed for internal analysis of the samples without compromising their structure. Scans were performed using a high-resolution industrial X-ray system, with carefully calibrated beam energy settings to ensure sufficient penetration and optimal image clarity of internal features.

The data obtained from the X-ray analysis provided complementary validation of the observations made during optical and SEM analysis. It also enabled a more holistic understanding of how casting defects vary by alloy composition and mold position, reinforcing the broader findings related to mechanical performance and defect distribution.

4

Results

4.1 Mechanical testing

4.1.1 Tensile testing

The results for F1 and F3 are discussed separately due to the different positions of these sections within the snake tool, which influences the mechanical properties.

F1 is positioned near the ingate, whereas F3 is located farther away, closer to the opposite end of the casting. Due to its longer flow length, F3 experiences faster cooling rate, but lower temperature when reaching filling. This faster cooling allows formation of more eutectic phases in F3. The presence of larger eutectic particles can potentially enhance the material's ductility and strength.

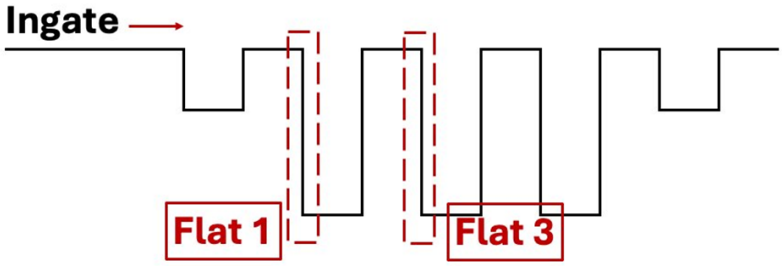

Figure 4.1: Position of flats F1 and F3 in the snake tool

This research aims to compare the results between different batches and positions. According to the Figure 4.2. A4 (primary ingots) serves as the baseline reference, exhibiting an average yield strength of approximately 113 MPa at position F1 and 117 MPa at position F3. B1 composed of secondary aluminum with high recycled content, displays YS values of 111 MPa (F1) and 123 MPa (F3) similar to A4. This suggests the recycled raw material, in this case, did not significantly alter the mechanical performance.

Meanwhile, B2 and B3 show a distinct improvement in yield strength. B2, with increased levels of Fe (0.3%), reached 120 MPa (F1) and 122 MPa (F3). This improvement is likely the result of solid solution strengthening, where the addition

of elements hinders dislocation movement and thereby increases the resistance to plastic deformation.

B3, which contains even higher Fe content (0.5%) along with 0.2% V, shows the highest average yield strengths: 135 MPa at F1 and 146 MPa at F3. The presence of V, even in small composition, likely contributes to precipitation hardening, promoting finer grain structures and enhanced mechanical strength.

When it comes to ultimate tensile strength (UTS) and elongation, A4 and B1 perform similarly. In F1, B2 and B3 have a worse performance, their UTS and elongation are noticeably lower compared to batch A4 and B1. However, in F3, B2 and B3 perform better, showing a significant boost compared to their results in F1 and outperforming A4 and B1 in the case of UTS.

These trends suggest that the location within the snake tool has a real impact on the UTS and elongation of the material. The better performance of B2 and B3 in F3 could be linked to differences in process parameters and how the material cooled or flowed during casting, affecting the internal structure and, ultimately, the mechanical properties.

Keeping the element content same and adjusting the secondary content in the alloy may not have a huge impact to the yield strength, UTS and elongation performance. The B1 batch which contains higher secondary aluminum can have a similar performance as A1 when their chemistry composition is same.

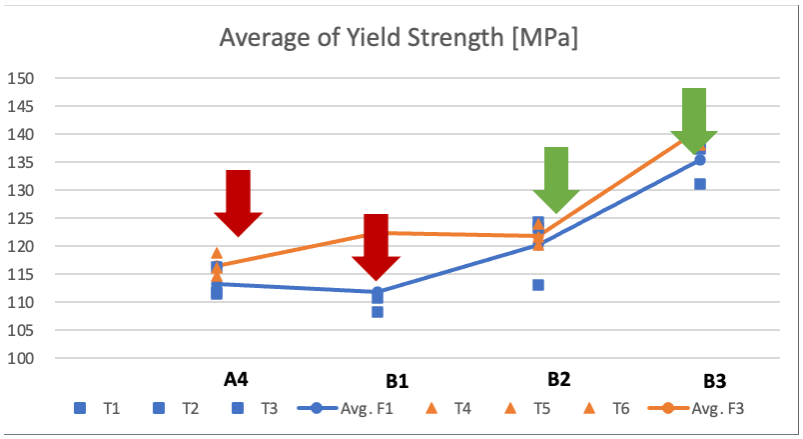

Figure 4.2: Avg. yield strength results: B1 exhibits a similar yield strength to A4 highlighted in red arrow, while both B2 and B3 show a noticeable increase highlighted in green arrow.

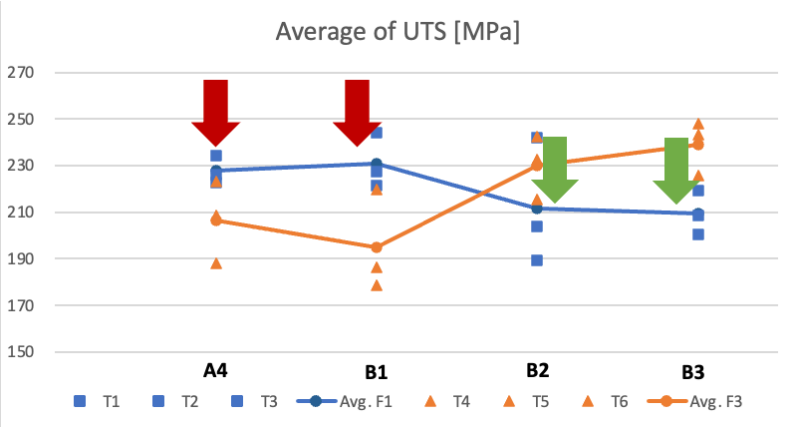

Figure 4.3: Avg UTS results: A4 and B1 have similar level of UTS. In Flat 1 (F1) highlighted in red arrow, B2 and B3 perform worse in both metrics. However, in Flat 3 (F3), B2 and B3 exhibit the opposite trend highlighted in green arrow

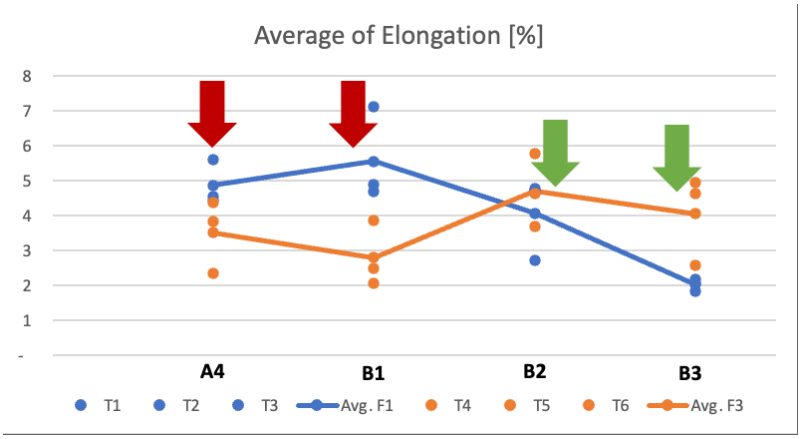

Figure 4.4: Avg elongation results: A4 and B1 have similar level of elongation highlighted in red arrow. In Flat 1 (F1), B2 and B3 perform worse in both metrics. However, in Flat 3 (F3), B2 and B3 exhibit the opposite trend highlighted in green arrow

Then the results were break down to another level. The six samples taken from the snake tool product are cut in different positions. T1 and T3 from F1 are vertical, and T2 is horizontal. Same as F3, T4 and T6 are vertical, and T5 is horizontal. Therefore, two other data comparison are conducted. The data is grouped by T1 & T3 and T4 & T6, T2 and T5. Based on the result in Figure 4.5, vertical samples have similar performance with the previous one. However, for horizontal samples, the UTS and elongation results of B3-T5 are higher than B3-T2, which are different from the previous results. Besides, the elongation at A4-T5 and B1-T5 are around 2%, which should pay more attention to.

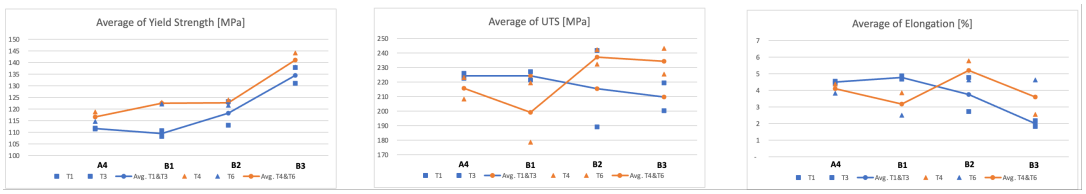

Avg YS, UTS and elongation results of T1 & T3 vs. T4 & T6

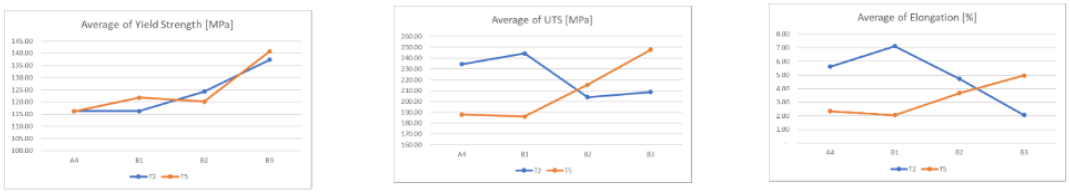

Avg YS, UTS and elongation results of T2 vs. T5

Figure 4.5: Avg YS, UTS and elongation results compared by horizontal and vertical direction samples: vertical samples have similar performance with the previous one. However, for horizontal samples, the UTS and elongation results of B3-T5 are higher than B3-T2, which are different from the previous results.

4.1.2 Bend plate test

A graph was created using the bending angles calculated for all the samples to get a clearer picture of how each one behaves under stress.

The graph shows the average bending angle for each batch across two positions. From the results it is evident that batches A4 and B1 exhibit comparable bending performance in both F1 and F3 positions, indicating similar ductility. Their relatively higher bending angles suggest that they can withstand more deformation before cracking.

In contrast, B2 and B3 show a noticeable reduction in bending angles at F1, implying decreased ductility and a higher tendency toward brittle behaviour. However, B3 shows a significant increase in bending performance at F3, nearly matching A4 and B1. This positional dependency suggests that process parameters such as localized cooling rates or material flow patterns during the HPDC process affect the final mechanical properties.

In summary, while A4 and B1 batches consistently perform similar, the performance of all the batches are highly position sensitive. This highlights the importance of uniform processing conditions to ensure consistent mechanical behaviour across different positions in the cast component.

4.1.2.1 Comparison - Tensile vs. Bending

Tensile tests are for understanding how a material handles stress in localized region, especially when looking at its resistance to permanent deformation. It apply a

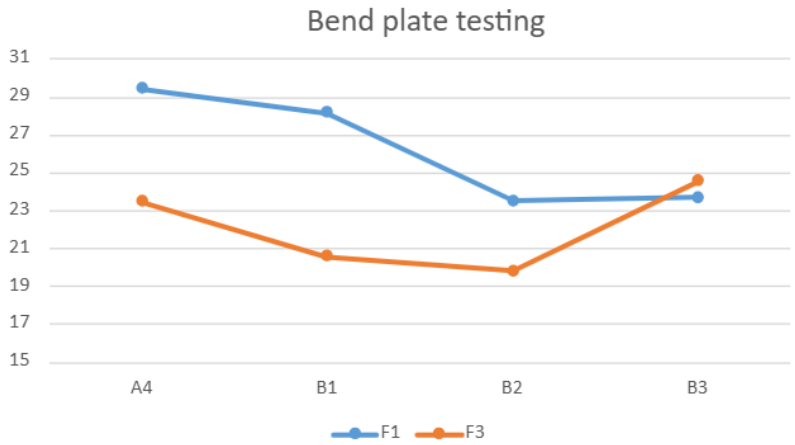

Figure 4.6: Bend plate test results: A4 and B1 show consistently higher bending angles at F1, indicating better ductility. B3 exhibit a huge increase in bending angle at F3, showing a position sensitive performance

nearly uniform stress across a large volume of material until failure. Statistically, this larger stressed volume has a higher probability of getting a critical defect, for instance, pores and cracks. That would make tensile results very sensitive to even small flaws.

In contrast, three-point bending tests take high stress in a much smaller volume near the load point, so the chance of hitting a huge defect is lower. Therefore, bending offers a clearer view of a material's overall ductility ability. In short, tensile testing highlights the impact of volumetric defects on strength, while bending testing can reflect better in-reality ductility under localized loading.

Based on the results of the average elongation and bending angles shows in Figure 4.7, a rough conclusion can be summarized that, A4 and B1 have similar performance, B2 and B3 have a lower performance on both tests. The results of both tests contain similar trend in every material batch.

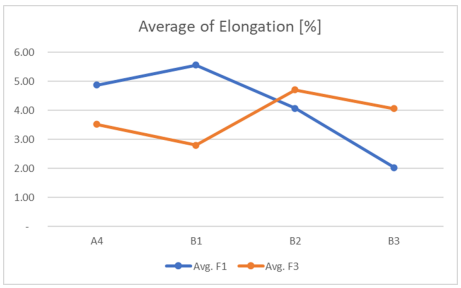

Avg elongation results of tensile test

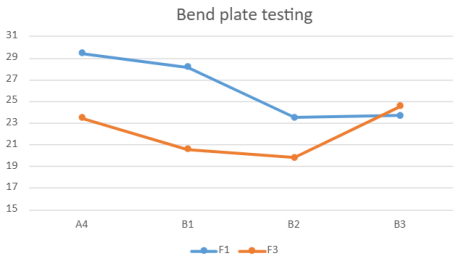

Bending test results

Figure 4.7: Tensile test results vs. Bending test results: Both results reflect A4 and B1 have similar performance, B2 and B3 perform relevantly poor.

4.1.2.2 Comparison – Flat sample vs Beam structure

To cross-check the findings, a comparison of results with another ongoing thesis [54] that focused on the U-beam structure used in the same snake tool was done. This gave a good reference point and made it easier to compare outcomes directly. A total 10 beam samples were used in this study for analysis.

Looking at the fracture surfaces Figure 4.8, a clear pattern was observed. Beam that fractured after shorter travel distances during bending tend to have smooth, flat surfaces. Hinting this might be more brittle failure, where the material breaks with very little plastic deformation.

However, beams that withstood higher travel distance before breaking showed much rougher and more irregular fracture surfaces. When observed, these samples had uneven textures and signs of plastic deformation, indicating more ductile failure. The middle structure of both beams show more rough and ductile surface.

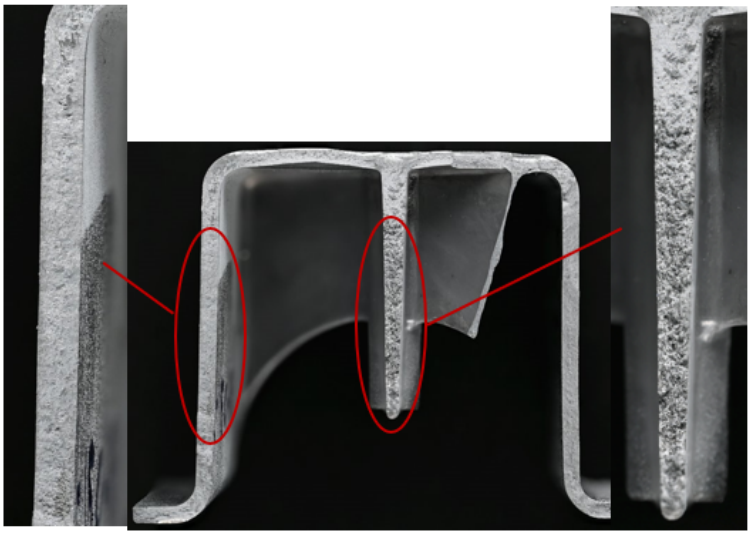

Beam A: Max travel distance of bending test: 48.84mm

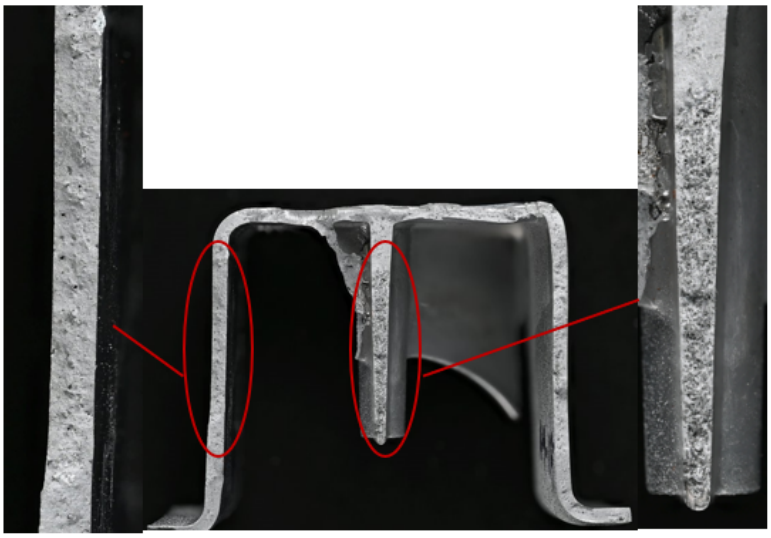

Beam B: Max travel distance of bending test: 22.22mm

Figure 4.8: Comparison of two fracture surface pictures of beam bending samples.

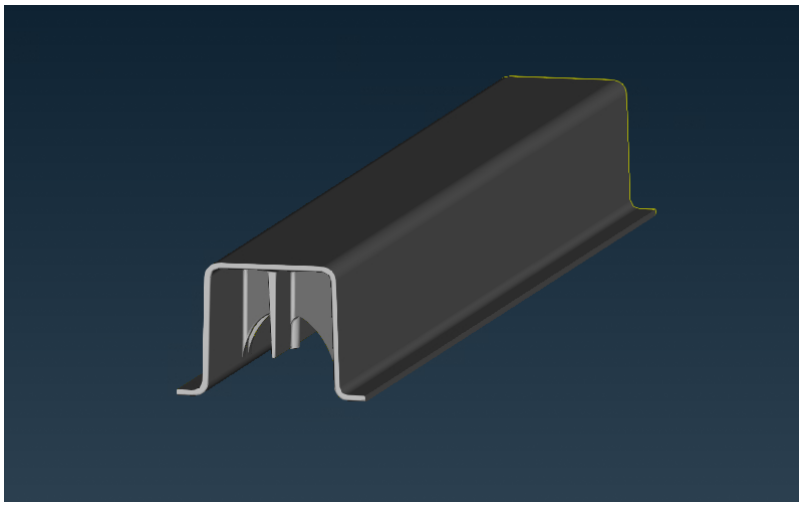

Figure 4.9: Beam structure

The bending test results of the flat samples were compared to those of the U-beam structure. In the flat bending test, the bending angle was measured, while in the beam bending test, the maximum travel distance was recorded, both providing a clear indication of each sample's toughness.

The results from both tests followed a similar pattern, showing consistent trends in toughness across the different materials. Samples B2 and B3 stood out for performing worse in both tests, which could likely be linked to their higher Fe content. Higher Fe levels are known to reduce ductility and make the material more prone to brittle failure, which explains the results observed.

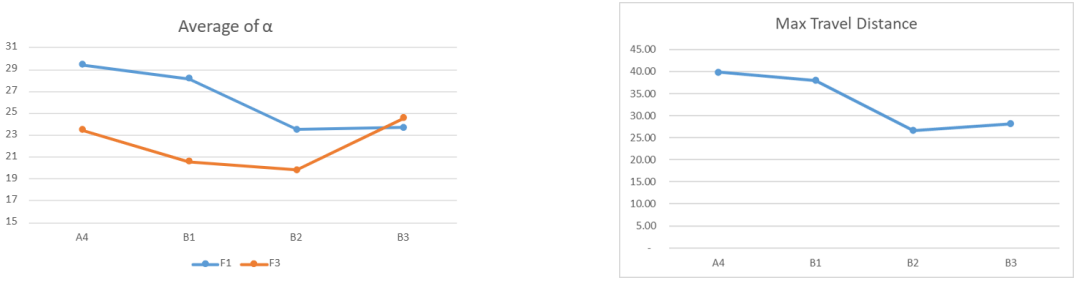

Flat bending results

Beam bending results

Figure 4.10: Flat & Beam bending results: Both bending test results show similar trend.

4.1.3 Hardness test

The hardness test results across the four batches shows relatively consistent values, with no major changes between positions F1 and F3. In F1 position, hardness values ranged from 80 HBW in A4 and B2, to 82 HBW in B1, and up to 84 HBW in B3. Similarly, in F3, hardness values increased gradually from 74 HBW in A4 to 78 HBW in B1, 80 HBW in B2, and again 84 HBW in B3. These results suggest that

the material maintains a stable hardness value across different batches, with B3 consistently demonstrating the highest values.

The minimal variation in hardness indicates that changes in chemical composition and the recycled material content do not have a major effect on the alloy's ability to resist indentation or deformation.

However, the addition of Fe and V have small but noticeable difference. These elements are known to strengthen materials by influencing the microstructure, so even though the change in hardness is not huge, it is likely that Fe and V contributed to a slight increase in hardness. This could be due to their role in forming stronger phases within the alloy, which helps it resist wear and deformation better than it would be without them.

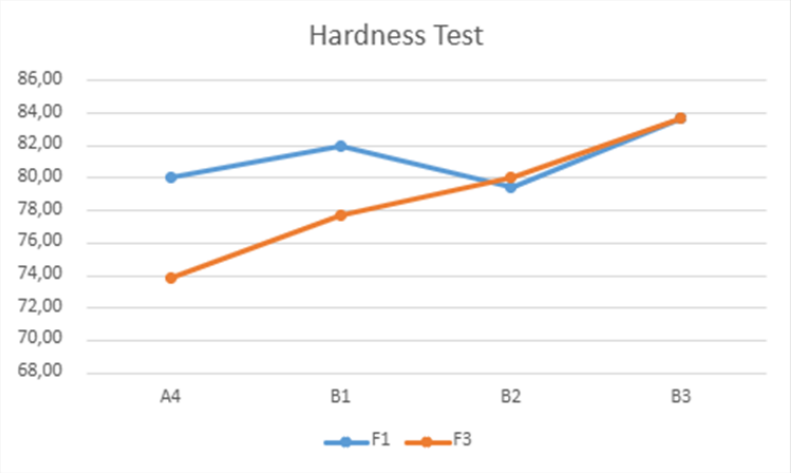

Figure 4.11: Hardness test results: Similar hardness results within all batches, secondary aluminum content and chemical composition do not affect significantly.

4.2 Fractography of tensile samples

4.2.1 Stereo microscopy

The fracture surface analysis of A4 and B1, reveals a noticeable concentration of porosity at the centre. These defects likely formed during solidification, possibly due to shrinkage or trapped gas both being common challenges in metal casting. Their presence points to the need for better control during the casting process, especially in terms of mold design and feeding systems, to help reduce internal voids and improve the overall reliability of the components.

Inspecting fracture surfaces from positions F1 and F3, a notable degradation in surface quality is observed in F3. F3 stands out with a higher number of defects, and these are not just more frequent but also larger and spread across the entire surface. This explains why F3 performs worse when it comes to ductility.

However, even with these defects, the fracture surfaces in all samples still show typical signs of ductile characteristics. The surfaces are rough, torn, and dimpled signs that show the material can absorb energy and deform rather than brittle fracture.

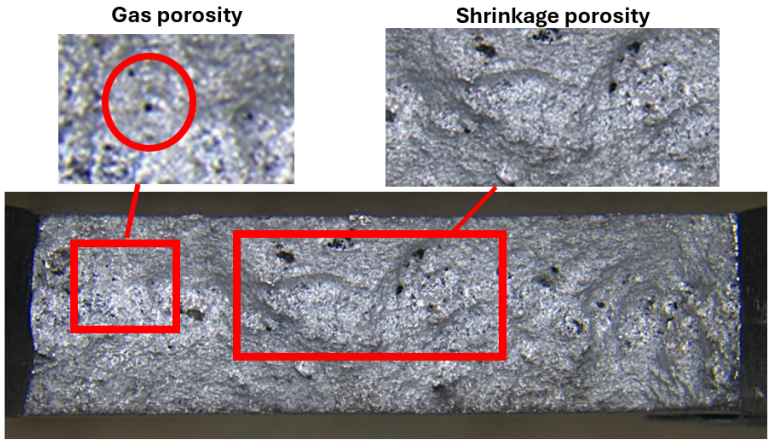

Figure 4.12: Example for gas porosity and shrinkage porosity

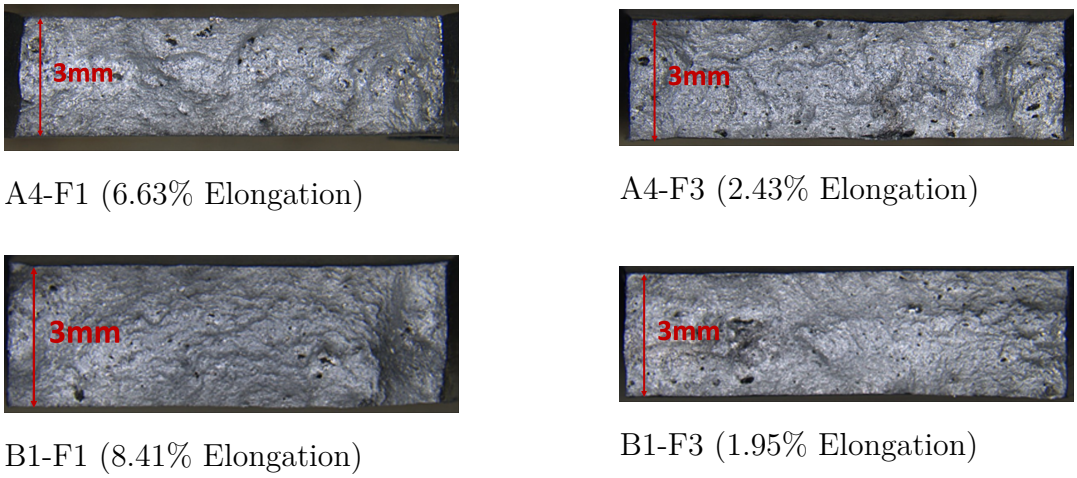

A4-F1 (6.63% Elongation)

A4-F3 (2.43% Elongation)

B1-F1 (8.41% Elongation)

B1-F3 (1.95% Elongation)

Figure 4.13: Microscopy pictures of A4 and B1 from F1 and F3 positions with elongation results

4.2.2 Metallography

Based on the shrinkage area percentage evaluated by Fiji software in Table 4.1, we can get the results of structure comparison.

In A4 and B1, the grain structures are finer and more evenly spread out compared to B2 and B3. This finer structure gives the material better ductility and strength, as small, evenly distributed grains help stop cracks from forming and spreading when the material is put under stress.

F3, however, has a lot more shrinkage cavities and casting defects than F1. These defects weaken the material by creating stress concentration for cracks to start,

which likely explains why F3 shows lower mechanical performance, especially when it comes to strength and ductility.

Another observation is the presence of larger aluminum grains in the F1 area. This is most likely because some of the molten metal began to solidify too early in the shot sleeve before being properly injected into the mold. When this early solidification occurs, it tends to produce coarser grains, which can make the material a little more brittle and less resistant to deformation.

Sample Name	**Shrinkage Area %**	**Elongation %**
A4-F1	0.205%	4.87%
A4-F3	0.830%	3.51%
B1-F1	0.148%	5.56%
B1-F3	0.640%	2.80%
B2-F1	0.811%	4.07%
B2-F3	1.902%	4.70%
B3-F1	0.594%	2.03%
B3-F3	0.729%	0.73%

Table 4.1: Shrinkage area percentage of different samples based on metallographic image analysis

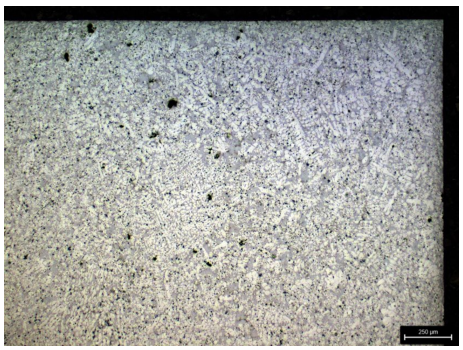

A4 - F1

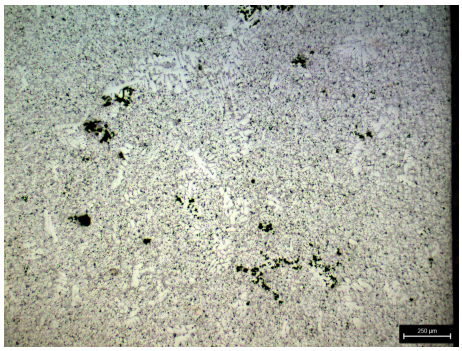

A4 - F3

A4 - F1

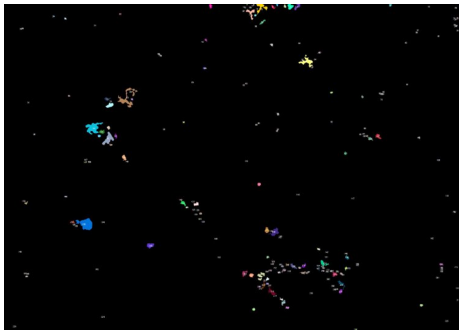

A4 - F3

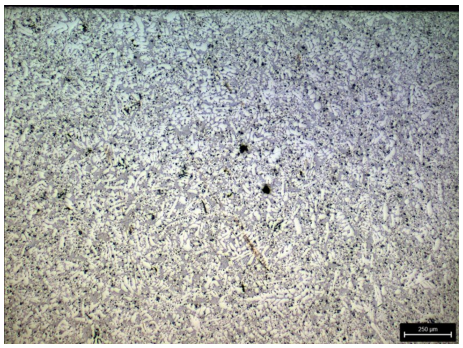

B1 - F1

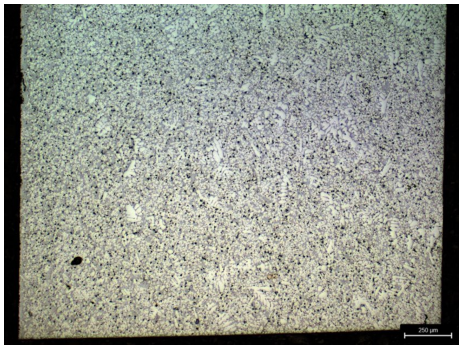

B1 - F3

B1 - F1

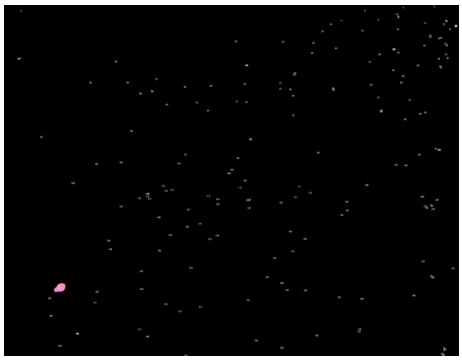

B1 - F3

Figure 4.14: Metallography and Fiji pictures of A4 and B1 batch from different positions

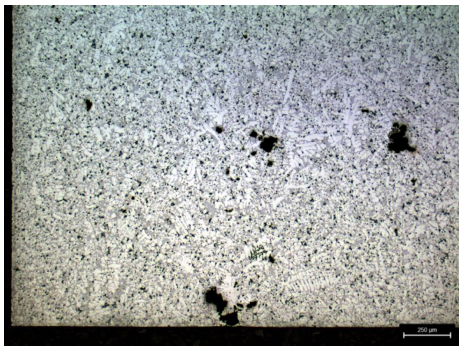

B2 - F1

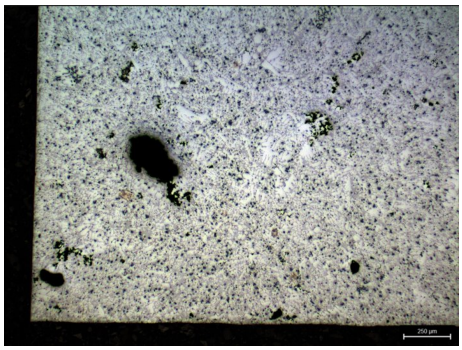

B2 - F3

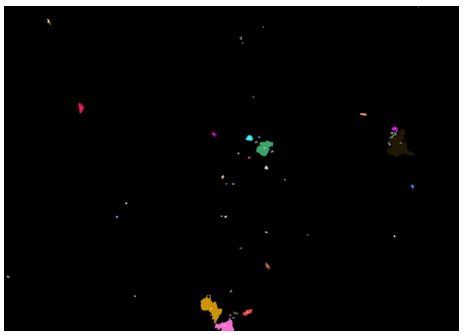

B2 - F1

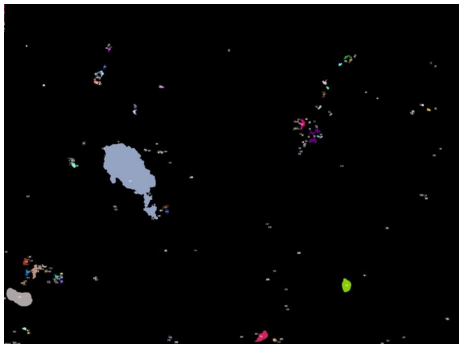

B2- F3

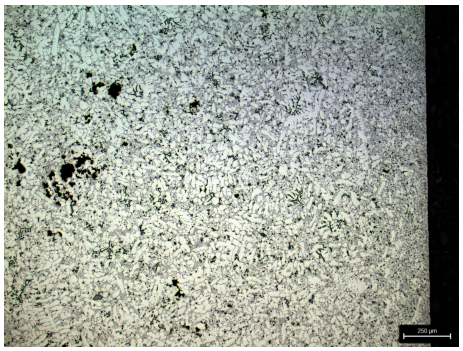

B3 - F1

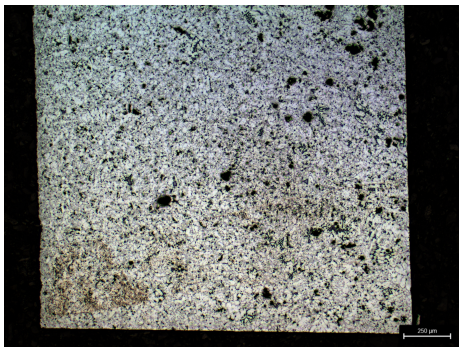

B3 - F3

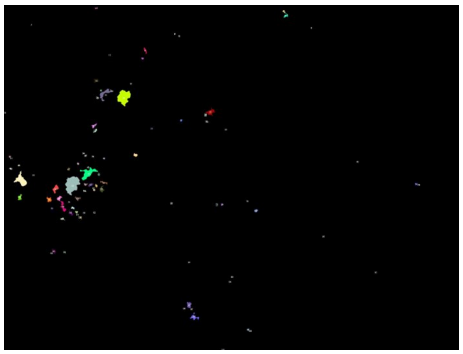

B3 - F1

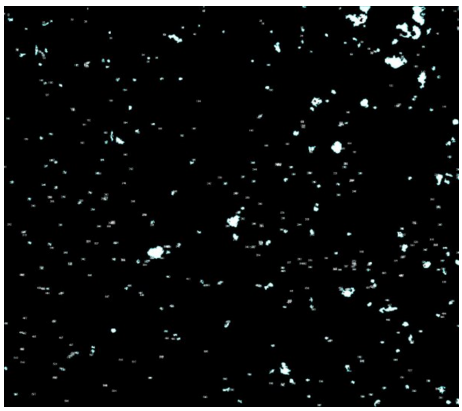

B3 - F3

Figure 4.15: Metallography and Fiji pictures of B2 and B3 batch from different positions

4.2.3 Comparison between snake tool and historical cast trial

The raw material in snake tool B1 and historical cast trial A3 was from the same raw material batch with the same chemical composition. The heat treatment status is different, snake tool includes paint baking, and the samples from historical cast trial are as cast. Comparing the microstructure and mechanical performance between these two batches gives a result to check the processing effect.

This comparison between snake tool B1 and the historical cast trial A3, even though both used the same raw material chemistry composition, shows how much the processing method can affect the final result. The historical cast sample had a much higher shrinkage area (1.300%) compared to snake tool B1 (0.148%), which was evaluated by Fiji. This means there were more internal voids and gaps formed during casting, which can weaken the part and make it more prone to failure under stress.

However, the grain structure of the aluminum phase in historical cast trial is much finer and more uniform. Smaller grain sizes are usually a good sign they often lead to stronger, tougher materials with better resistance to wear and deformation. So, even though historical cast had more shrinkage defects, its finer microstructure improved the mechanical properties. In contrast, the snake tool sample showed fewer defects but had a coarser grain structure. While this might reduce internal flaws, it also limits how strong or durable the part can be.

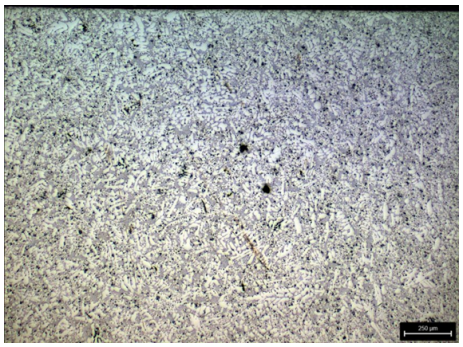

Snake tool microstructure shrinkage area%: 0.148%

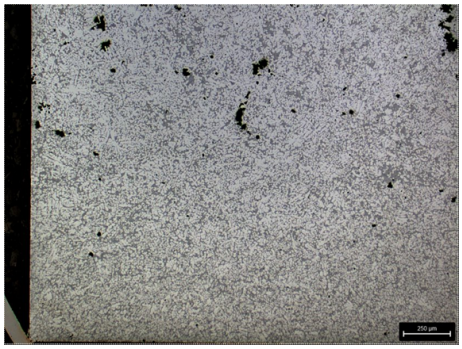

historical cast trials microstructure shrinkage area%: 1.300%

Figure 4.16: Comparison of shrinkage area between snake tool and historical cast trials microstructure

Even though the snake tool B1 and historical cast trial A3 samples had some differences in their microstructure, their overall mechanical properties like yield strength, tensile strength, elongation, and hardness ended up being quite similar.

What really stands out is the bending performance. Despite the historical cast trial having a much higher shrinkage area (1.300%) compared to snake tool (0.148%), it performed better in the bending test, reaching a larger bending angle. One possible

reason for this is that most of the deformation during bending may have taken place away from the main zone of shrinkage defects.

Sl.no	Objective	Snake tool B1 (paint bake)	historical cast trial A3 (as cast)
1	Shrinkage area%	0.148%	1.300%
2	Thickness	3mm	4mm
3	Tensile,YS(MPa)	112	125
4	Tensile,UTS(MPa)	231	240
5	Tensile,Elongation%	5.6%	5.7%
6	Bending test °,	28.19°	37.37°
7	Hardness, HBW	82	72

Table 4.2: Comparison between Snake tool and historical cast trial

4.2.4 SEM

Once comparing the different material batches, B1 shows a clear increase in the number of large intermetallic particles compared to A4, indicating the influence of recycled material. This trend is more noticeable in B2 and B3, where not only are there more intermetallic particles, but they are also significantly larger.

Additionally, B2 and B3 exhibit a higher concentration of distinct morphological features, particularly blocky and script-shaped intermetallic phases. Altogether, these changes point to a gradual shift in the alloy's structure, caused by differences in composition and increase in iron percentage and how the material solidifies during casting.

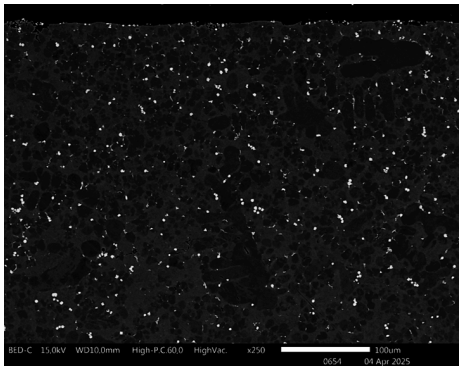

A4 - F1

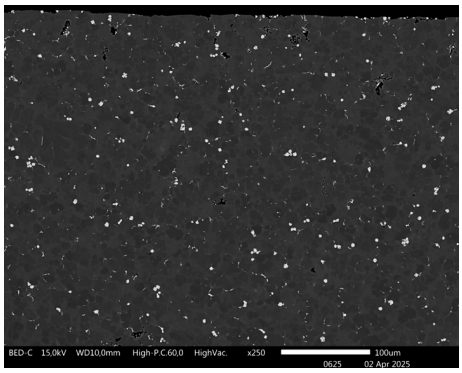

A4 - F3

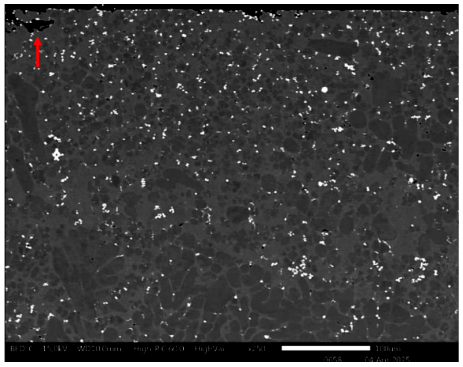

B1 - F1

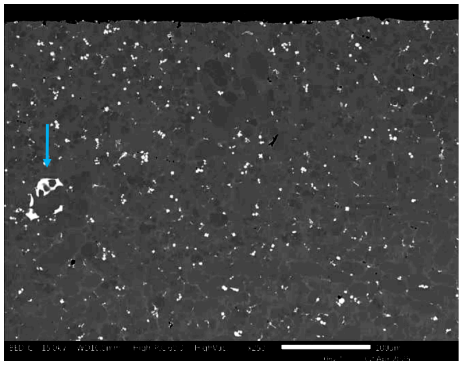

B1 - F3

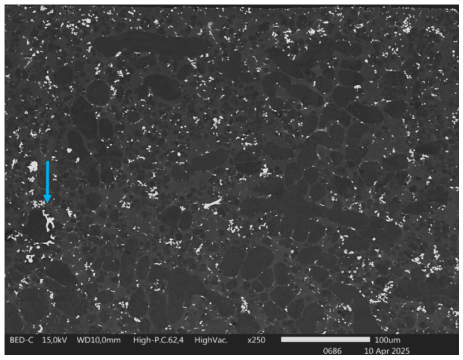

B2 - F1

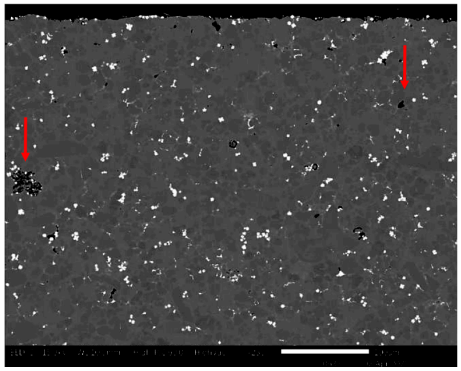

B2 - F3

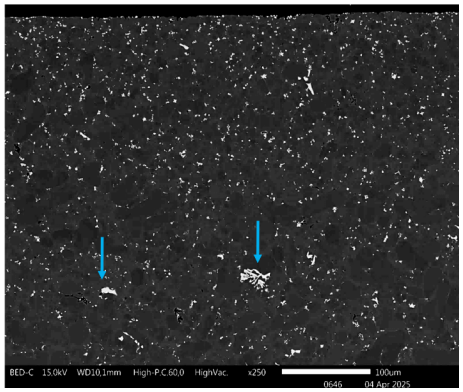

B3 - F1

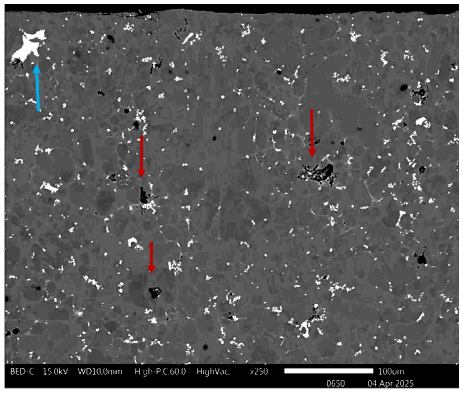

B3 - F3

Figure 4.17: SEM pictures of all batches and different positions, red arrow highlights: porosity, blue arrow highlights: blocky and script scaped phases

4.2.5 X-ray

When compared with the same positions, X-ray analysis indicates that sample B2 contains a significantly higher number of cracks and internal defects compared to B1 and A4, pointing to potential inconsistencies in composition or casting conditions. When compared with different positions, the surface of F3 displays more visible defects than F1. These findings are consistent with the results obtained from metallographic analysis and mechanical testing, all of which highlight a recurring trend.

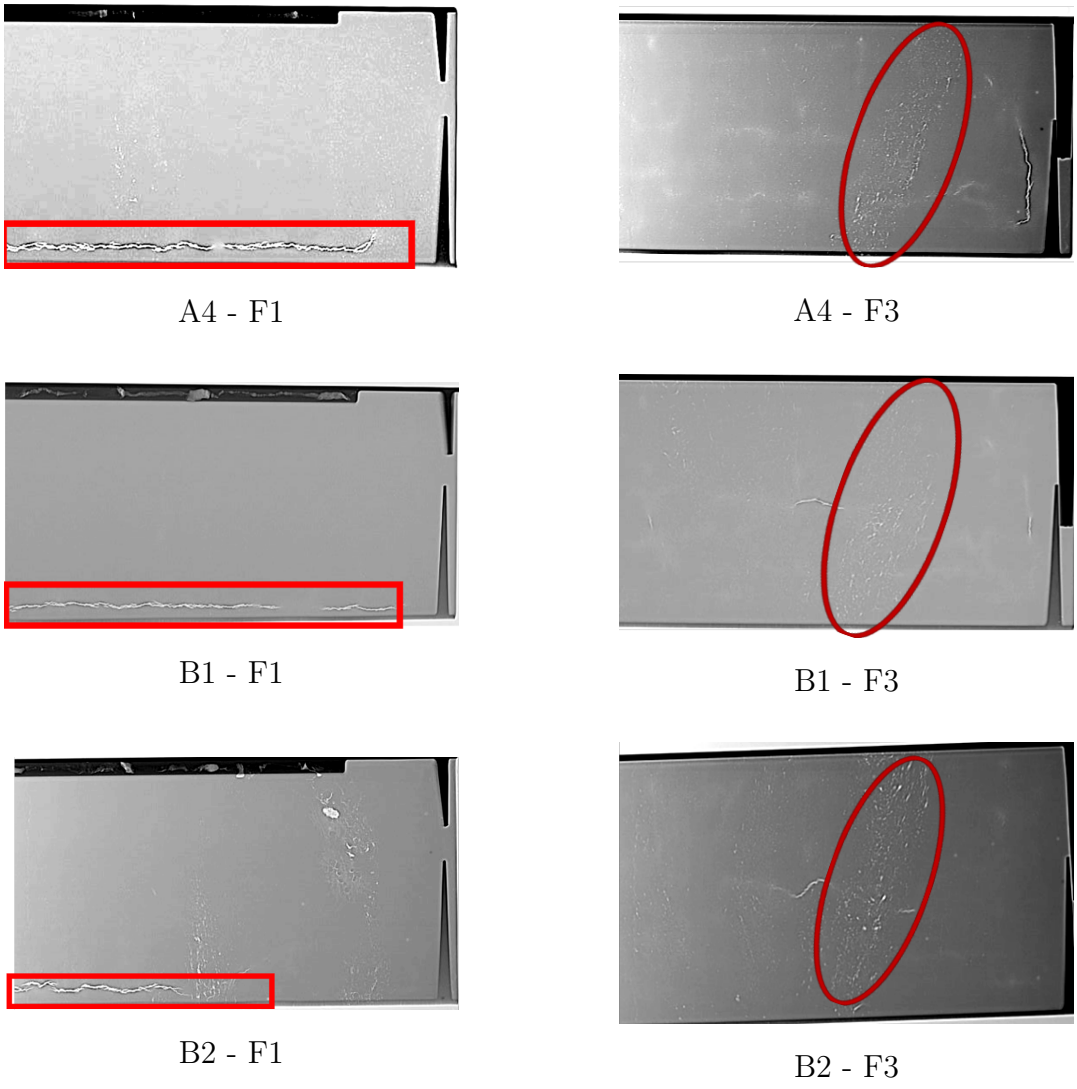

Figure 4.18: X-ray pictures of A4, B1 and B2 batches

4.2.6 Effect of chemical composition and process parameters

In this study, it is essential to distinguish the effects of chemical composition from those caused by process parameters.

4.2.6.1 Impact of chemical composition

To differentiate the effects of alloy chemistry from processing conditions, samples with similar chemical compositions but different sources of aluminum were first examined. A4, produced using primary aluminum, and B1, produced using high recycled content, share nearly identical chemical compositions. Both exhibited comparable levels of shrinkage and surface defects, although B1 presents a greater quantity and size of intermetallic phases. As Fe content increased from 0.2% to 0.3% (B2), both the shrinkage area and the number of script- and blocky-shaped intermetallics increased. Further increasing Fe to 0.5% and introducing 0.2% V (B3) led to a reduction in shrinkage and intermetallic size compared to B2, but still higher than A4 and B1. These microstructural differences closely align with mechanical performance: A4 and B1 exhibit comparable properties, while B2 and B3 demonstrate increased yield strength but reduced UTS and ductility.

4.2.6.2 Impact of process conditions

The influence of process conditions was analyzed by comparing samples from different positions within the snake tool, Flat 1 (F1) and Flat 3 (F3). Due to their relative locations, F3 samples experience a longer flow length, leading to a lower melt temperature and higher cooling rate upon mold filling. As a result, F3 samples showed more large shrinkage, oxide formation, larger intermetallic phases, and more visible surface irregularities. These microstructural differences correlate with mechanical performance: F3 samples had higher yield strength, likely due to increased eutectic content, but lower ductility compared to F1, which contained a higher proportion of α-aluminum phase.

These findings support the conclusion that both alloy composition and process conditions independently and jointly influence the formation of casting defects and the mechanical response of HPDC aluminum alloys.

5

Conclusion

1. This study demonstrates that aluminum alloys with up to 90% recycled content (B1) can deliver mechanical performance comparable to primary aluminum (A4), and the alloy composition keeps on the same level. Batch B2 and B3 have similar performance in every mechanical tests, however, they exhibited higher yield strength and UTS but reduced ductility, suggesting a trade-off influenced by the addition of Fe and V.

2. The positional differences observed between F1 and F3 emphasize how positions, local thermal and flow conditions during HPDC can significantly affect shrinkage, defect formation, reflecting mainly on ductility. General conclusions underline the need for targeted process optimization, particularly in complex casting geometries like those used in megacasting.

3. Hardness measurements remained relatively stable across all batches and positions, indicating that moderate variations in alloy composition had limited influence on resistance to indentation.

4. Metallographic analysis revealed that A4 and B1 possessed finer and more uniform grain structures compared to B2 and B3. Samples with longer flow length (F3) consistently showed larger shrinkage areas and casting defects than ones with shorter flow length (F1), correlating with their reduced ductility performance.

5. SEM observations confirmed a progressive increase in the size and quantity of intermetallic phases from A4 to B3. In particular, B2 and B3 contained coarse, blocky, and script-shaped intermetallics, which are associated with lower ductility.

6. X-ray shows more internal defects in the samples with Fe 0.3% (B2) and samples with longer flow length (F3).

7. Compositional variations, particularly increased Fe and V content (B2 (Fe 0.3%, V 0.01 %) and B3 (Fe 0.5%, V 0.2%)), were associated with greater shrinkage and intermetallic formation than samples with lower Fe and V content (A4&B1 (Fe 0.2%, V 0.01 %)). Additionally, longer flow lengths (F3) led

to lower temperatures and faster cooling, causing more shrinkage and intermetallic formation than shorter flow lengths (F1).

8. The use of the snake tool proved effective in evaluating casting behavior and mechanical performance across different positions. Its intricate geometry and downsized mold format enabled early identification of casting-related defects and material weaknesses, offering an efficient and material-saving approach to assess the viability of alloys and process parameters before full-scale production. However, process challenges during casting seems to have significant effect on the material properties.

9. Overall, this study supports the implementation of recycled aluminum in structural megacasting components. When alloy chemistry of recycled alloys such as B1 was the same chemical composition as primary aluminum, and keeps the same cast processing parameters, the recycled alloys can provide a sustainable and high-performing alternative to primary aluminum in automotive applications. When the Fe content is raised to 0.3% (B2), the yield strength remains comparable to that of the secondary alloy with 0.2% Fe (B1). However, B2's UTS and elongation vary more markedly with position, it performs worse than B1 at the shorter flow-length region (F1) but outperforms B1 at the longer flow-length region (F3). In bending, B2 shows slightly lower ductility than B1. The alloy containing 0.5% Fe and 0.2% V (B3) achieves the highest yield strength of all batches. Longer flow length leads to lower temperatures and faster cooling, causing more shrinkage and intermetallic formation.

6

Next Steps & Recommendation

1. While the snake tool offers valuable insight, follow-up validation using full-scale automotive parts under industrial conditions would enhance result relevance on component level.

2. Implement a statistically robust experimental design with increased sample numbers, randomized position sampling (F1 vs. F3), and appropriate statistical analyses to quantify and validate the position-sensitivity of defect formation and mechanical performance.

3. Future studies could apply quantitative SEM/EDS and EBSD to better characterize intermetallic types, grain orientations, and crack initiation mechanisms.

4. Explore alternative gate design, plunger speed profiles, and improves vacuum to reduce process defects like shrinkage and gas porosity, especially improving cast quality in areas with long flow length.

5. Since this work ties into Volvo Car's sustainability goals, integrating a life-cycle analysis (LCA) of each alloy batch would provide a solid evaluation of environmental benefits versus technical risks.

6. Alloys with added Fe and V (like B3) showed improved strength but reduced ductility. Trade-offs like this can be evaluated with modified material card in CAE simulations before implementation in real components.

Bibliography

[1] ACEA, *Co2 emissions from car production in the eu*, Online article, Accessed: 2024-01-16, 2023. [Online]. Available: https://www.acea.auto/figure/co2-emissions-from-car-production-in-eu/.

[2] EPA, *Biden-harris administration finalizes strongest ever greenhouse gas standards for heavy-duty vehicles to protect public health and address the climate crisis while keeping the american economy moving*, Online article, Accessed: 2025-02-03, 2024. [Online]. Available: https://www.epa.gov/newsreleases/biden-harris-administration-finalizes-strongest-ever-greenhouse-gas-standards-heavy.

[3] C. of the EU, *'fit for 55': Council adopts regulation on co2 emissions for new cars and vans*, Online article, Accessed: 2025-02-03, 2023. [Online]. Available: https://www.consilium.europa.eu/en/press/press-releases/2023/03/28/fit-for-55-council-adopts-regulation-on-co2-emissions-for-new-cars-and-vans/.

[4] Reuters, *Tesla working on 'gigacasting' tech to mould underbody in one piece, shanghai securities news reports*, Online article, Accessed: 2025-02-03, 2023. [Online]. Available: https://www.reuters.com/business/autos-transportation/tesla-shanghai-plant-starts-model-y-production-with-new-cost-cutting-methods-2023-09-27/.

[5] A. M. C. GmbH, "Market overview giga casting and giga presses in the automotive industry," ANP Management Consulting GmbH, Tech. Rep., 2024, Accessed: 2025-02-03. [Online]. Available: https://www.anp-consulting.com/wp-content/uploads/2024/01/Gigacasting-Megacasting-Update-Jan-2024.pdf.

[6] A. Hartlieb and M. Hartlieb, *The impact of giga-castings on car manufacturing and aluminum content*, Online article, Accessed: 2025-02-03, 2023. [Online]. Available: https://www.lightmetalage.com/news/industry-news/automotive/the-impact-of-giga-castings-on-car-manufacturing-and-aluminum-content.

[7] H. Baker and H. Okamoto, "Asm handbook: Volume 3: Alloy phase diagrams asm international," *Materials Park*, 1992.

[8] J. A. Taylor, "Iron-containing intermetallic phases in al-si based casting alloys," *Procedia Materials Science*, vol. 1, pp. 19–33, 2012.

[9] C.-L. Chen, A. Richter, and R. Thomson, "Investigation of mechanical properties of intermetallic phases in multi-component al–si alloys using hot-stage

nanoindentation," *Intermetallics*, vol. 18, no. 4, pp. 499–508, 2010, ISSN: 0966-9795. DOI: https://doi.org/10.1016/j.intermet.2009.09.013. [Online]. Available: https://www.sciencedirect.com/science/article/pii/S0966979509002635.

[10] M. Warmuzek, *Aluminum-silicon casting alloys: an atlas of microfractographs*. ASM international, 2004.

[11] N. U. O.S.I. Fayomi A.P.I. Popoola, "Effect of alloying element on the integrity and functionality of aluminium-based alloy," in *Aluminium Alloys - Recent Trends in Processing, Characterization, Mechanical Behavior and Applications*, 2017.

[12] A. D. Toni Bogdanoff Salem Seifeddine, "The effect of si content on microstructure and mechanical properties of al-si alloy," *La Metallurgia Italiana*, vol. 108, no. 6, pp. 65–69, 2016.

[13] J. N. I. Polmear D. Stjohn, "Wrought aluminium alloys," *Light Alloys (Fifth Edition)*, pp. 157–263, 2017. DOI: 10.1016/B978-0-08-099431-4.00004-X.

[14] X. Liu, C. Wang, S.-Y. Zhang, *et al.*, "Fe-bearing phase formation, microstructure evolution, and mechanical properties of al-mg-si-fe alloy fabricated by the twin-roll casting process," *Journal of Alloys and Compounds*, vol. 886, p. 161 202, 2021.

[15] M. Furui, T. Kitamura, T. Ishikawa, S. Ikeno, S. Saikawa, and N. Sakai, "Evaluation of age hardening behavior using composite rule and microstructure observation in al-si-mg alloy castings," *Materials transactions*, vol. 52, no. 6, pp. 1163–1167, 2011.

[16] G. Thompson, "The role of alloying elements on the surface treatment and finishing of aluminium," *Materials Science Forum*, vol. 519-521, pp. 615–620, 2006. DOI: 10.4028/www.scientific.net/MSF.519-521.615.

[17] D. Stanić, Z. Zovko Brodarac, and L. Li, "Influence of copper addition in alsi7mgcu alloy on microstructure development and tensile strength improvement," *Metals*, vol. 10, no. 12, p. 1623, 2020.

[18] M. T. Di Giovanni, E. A. Mørtsell, T. Saito, *et al.*, "Influence of cu addition on the heat treatment response of a356 foundry alloy," *Materials Today Communications*, vol. 19, pp. 342–348, 2019.

[19] J. Baskaran, P. Raghuvaran, and S. Ashwin, "Experimental investigation on the effect of microstructure modifiers and heat treatment influence on a356 alloy," *Materials Today: Proceedings*, vol. 37, pp. 3007–3010, 2021.

[20] E. Wang, X. Hui, S. Wang, Y. Zhao, and G. Chen, "Improved mechanical properties in cast al–si alloys by combined alloying of fe and cu," *Materials Science and Engineering: A*, vol. 527, no. 29-30, pp. 7878–7884, 2010.

[21] M. Valsange, S. Kulkarni, and S. Sonawane, "Stir casting used in manufacturing of aluminium matrix composite," *International Journal for Research in Technological Studies*, vol. 1, no. 9, pp. 35–38, 2014.

[22] V. Bharath, M. Nagaral, V. Auradi, and S. Kori, "Preparation of 6061al-al2o3 mmc's by stir casting and evaluation of mechanical and wear properties," *Procedia materials science*, vol. 6, pp. 1658–1667, 2014.

[23] K. Sankaran and R. Mishra, "Chapter 4 – aluminum alloys," pp. 57–176, 2017. DOI: 10.1016/B978-0-12-812068-2.00004-7.

[24] A. Jarfors, A. Du, G. Yu, J. Zheng, and K. Wang, "On the sustainable choice of alloying elements for strength of aluminum-based alloys," *Sustainability*, 2020. DOI: 10.3390/su12031059.

[25] R. G. Bhandare, P. M. Sonawane, *et al.*, "Preparation of aluminium matrix composite by using stir casting method," *International Journal of Engineering and Advanced Technology (IJEAT)*, vol. 3, no. 3, pp. 61–65, 2013.

[26] A. Dahle, K. Nogita, S. McDonald, J. Zindel, and L. Hogan, "Eutectic nucleation and growth in hypoeutectic al-si alloys at different strontium levels," *Metallurgical and Materials Transactions A*, vol. 32, pp. 949–960, 2001.

[27] D. R. Consulting, "Aluminum content in passenger vehicles (europe)," European Aluminium, Tech. Rep., 2023, Accessed: 2025-02-05. [Online]. Available: https://european-aluminium.eu/wp-content/uploads/2023/05/2023_04_Aluminum-Content_Ducker-Study_EA-Public-Summary_190423.pdf.

[28] J. B. W.S. Miller L Zhuang, "Recent development in aluminium alloys for the automotive industry," *Materials Science and Engineering*, vol. 280, no. 1, pp. 37–49, 2000. DOI: 10.1016/S0921-5093(99)00653-X.

[29] E. Aluminium, "Materials designation system," 2002.

[30] J. Kaufman, "Properties and applications of wrought aluminum alloys," *ASM Handbook*, vol. 2B, pp. 202–275, 2019. DOI: 10.31399/asm.hb.v02b.a0006543.

[31] P. J. G.B. Burger A.K. Gupta, "Microstructural control of aluminum sheet used in automotive applications," *Materials Characterization*, vol. 35, no. 1, pp. 23–39, 1995. DOI: 10.1016/1044-5803(95)00065-8.

[32] E. Aluminium, "Aluminium usage in cars surges as automotive industry shifts towards electrification," 2023. [Online]. Available: https://european-aluminium.eu/wp-content/uploads/2023/05/23-05-02-European-Aluminium_PR_Aluminium-Usage-in-Cars-Surges-as-Automotive-Industry-Shifts-Towards-Electrification.pdf.

[33] "Stiffness relevance and strength relevance in crash of car body components," 2010. [Online]. Available: https://api.semanticscholar.org/CorpusID:148562905.

[34] R. Alloys, "Hpdc alloys for structural casts in vehicle construction," 2018. [Online]. Available: https://rheinfelden-alloys.eu/wp-content/uploads/2018/09/rheinfelden_alloys_structural_casts_2018.pdf.

[35] B. Callegari, T. N. Lima, and R. S. Coelho, "The influence of alloying elements on the microstructure and properties of al-si-based casting alloys: A review," *Metals*, vol. 13, no. 7, p. 1174, 2023.

[36] S. K. Das, J. A. Green, J. G. Kaufman, D. Emadi, and M. Mahfoud, "Aluminum recycling—an integrated, industrywide approach," *JOM*, vol. 62, pp. 23–26, 2010.

[37] K. Buxmann, "Ecological aspects of the use of aluminium in cars, with particular regard to recycling techniques," *Resources, Conservation and Recycling*, vol. 10, no. 1-2, pp. 17–23, 1994.

[38] Hydro, *Aluminium life cycle*, Online article, Accessed: 2025-02-12, 2025. [Online]. Available: https://www.hydro.com/en/global/aluminium/about-aluminium/aluminium-life-cycle/.

[39] R. Modaresi and D. B. Müller, "The role of automobiles for the future of aluminum recycling," *Environmental science & technology*, vol. 46, no. 16, pp. 8587–8594, 2012.

[40] S. K. Das and W. Yin, "The worldwide aluminum economy: The current state of the industry," *Jom*, vol. 59, pp. 57–63, 2007.

[41] I. Aluminium, *Primary aluminium smelting energy intensity*, Online article, Accessed: 2025-02-12, 2025. [Online]. Available: https://international-aluminium.org/statistics/primary-aluminium-smelting-energy-intensity/?publication=primary-aluminium-smelting-energy-intensity.

[42] M. da Silva, J. Pujante, J. Hrabia-Wiśnios, *et al.*, "Analysis of inclusions and impurities present in typical hpdc, stamping and extrusion alloys produced with different scrap levels," *Metals*, 2024. DOI: 10.3390/met14060626.

[43] J. A. Green, *Aluminum recycling and processing for energy conservation and sustainability*. ASM International, 2007.

[44] S. K. Padamata, A. Yasinskiy, and P. Polyakov, "A review of secondary aluminum production and its byproducts," *Jom*, vol. 73, no. 9, pp. 2603–2614, 2021.

[45] sphericalinsights, *Global aluminum scrap recycling market size*, Online article, Accessed: 2025-04-28, 2022. [Online]. Available: https://www.sphericalinsights.com/reports/aluminum-scrap-recycling-market.

[46] R. F. F. Casarotto A.J. Franke, "High-pressure die-cast (hpdc) aluminium alloys for automotive applications," *Advanced Materials in Automotive Engineering*, pp. 109–149, 2012. DOI: 10.1533/9780857095466.109.

[47] N. G. F. Bonollo and G. Timelli, "High-pressure die-casting: Contradictions and challenges," *JOM: the journal of the Minerals, Metals Materials Society*, vol. 67, no. 5, pp. 901–908, 2015. DOI: 10.1007/s11837-015-1333-8.

[48] K. Wärmefjord, J. Hansen, and R. Söderberg, "Challenges in geometry assurance of megacasting in the automotive industry," *Journal of Computing and Information Science in Engineering*, vol. 23, no. 6, p. 060 801, 2023.

[49] M. Ghomashchi, "High-pressure die casting: Effect of fluid flow on the microstructure of lm24 die-casting alloy," *Journal of Materials Processing Technology*, vol. 52, no. 2-4, pp. 193–206, 1995. DOI: 10.1016/0924-0136(94)01583-M.

[50] B. F. D.R. Gunasegaram and F. Polivka, "Melt flow velocity in high pressure die casting: Its effect on microstructure and mechanical properties in an al–si alloy," *Materials Science and Technology*, vol. 23, no. 7, pp. 847–856, 2007. DOI: 10.1179/174328407X176992.

[51] L. Bennett, *What is the high pressure die casting (hpdc) process*, Online article, Accessed: 2025-02-17, 2022. [Online]. Available: https://www.rapiddirect.com/blog/what-is-high-pressure-die-casting/.

[52] I. Precision, *Heat treatment for aluminum castings*, Online article, Accessed: 2025-02-18, 2022. [Online]. Available: https://www.improprecision.com/heat-treatment-aluminum-castings/.

[53] T. Cast, *Heat treatment for aluminum castings*, Online article, Accessed: 2025-02-18, 2021. [Online]. Available: https://tpicast.com/heat-treatment-for-aluminum-castings/.

[54] L. L. Melvin J, “Cae modeling of hpdc aluminum,” 2025.

DEPARTMENT OF SOME SUBJECT OR TECHNOLOGY
CHALMERS UNIVERSITY OF TECHNOLOGY
Gothenburg, Sweden
www.chalmers.se

CHALMERS
UNIVERSITY OF TECHNOLOGY